Mechanical Characterization of Lithium-Ion Battery Micro Components for Development of Homogenized and Multilayer Material Models

By

Kyle M. Miller

Bachelor of Science in Systems Engineering,
United States Naval Academy, 2008

Submitted to the Department of Mechanical Engineering
in Partial Fulfillment of the Requirements for the Degrees of

Naval Engineer

And

Masters of Science in Mechanical Engineering

at the
Massachusetts Institute of Technology
June 2014

© 2014 Kyle M. Miller. All rights reserved

The author hereby grants to MIT permission to reproduce and to distribute publicly paper and electronic copies of this thesis document in whole or in part in any medium now known or hereafter created.

Signature of Author_____
Kyle M. Miller
Department of Mechanical Engineering
May 10, 2014

Certified by_____
Tomasz Wierzbicki
Professor of Mechanical Engineering
Thesis Supervisor

Accepted by_____
David E. Hardt
Chair, Departmental Committee on Graduate Students
Department of Mechanical Engineering

(This Page is Intentionally Left Blank)

REPORT DOCUMENTATION PAGE

Form Approved
OMB No. 0704-0188

The public reporting burden for this collection of information is estimated to average 1 hour per response, including the time for reviewing instructions, searching existing data sources, gathering and maintaining the data needed, and completing and reviewing the collection of information. Send comments regarding this burden estimate or any other aspect of this collection of information, including suggestions for reducing the burden, to Department of Defense, Washington Headquarters Services, Directorate for Information Operations and Reports (0704-0188), 1215 Jefferson Davis Highway, Suite 1204, Arlington, VA 22202-4302. Respondents should be aware that notwithstanding any other provision of law, no person shall be subject to any penalty for failing to comply with a collection of information if it does not display a currently valid OMB control number.
PLEASE DO NOT RETURN YOUR FORM TO THE ABOVE ADDRESS.

1. REPORT DATE *(DD-MM-YYYY)*	2. REPORT TYPE	3. DATES COVERED *(From - To)*
	Master's Thesis	15 May 2011-15 Jun 2014

4. TITLE AND SUBTITLE
Mechanical Characterization of Lithium-Ion Battery Micro Components for Development of Homogenized and Multilayer Material Models

5a. CONTRACT NUMBER
N00244-09-G0014

5b. GRANT NUMBER

5c. PROGRAM ELEMENT NUMBER

6. AUTHOR(S)
Kyle M. Miller

5d. PROJECT NUMBER

5e. TASK NUMBER

5f. WORK UNIT NUMBER

7. PERFORMING ORGANIZATION NAME(S) AND ADDRESS(ES)
Massachusetts Institute of Technology

8. PERFORMING ORGANIZATION REPORT NUMBER

9. SPONSORING/MONITORING AGENCY NAME(S) AND ADDRESS(ES)
Naval Postgraduate School
Monterey, CA 93943

10. SPONSOR/MONITOR'S ACRONYM(S)
NPS

11. SPONSOR/MONITOR'S REPORT NUMBER(S)

12. DISTRIBUTION/AVAILABILITY STATEMENT
Approved for public release; distribution is unlimited.

13. SUPPLEMENTARY NOTES

14. ABSTRACT
The overall battery research of the Impact and Crashworthiness Laboratory (ICL) at MIT has been focused on understanding the battery's mechanical properties so that individual battery cells and battery packs can be characterized during crash events. The objective of this research is to better understand the battery component (electrode and separator) properties under different loading conditions.

15. SUBJECT TERMS

16. SECURITY CLASSIFICATION OF:			17. LIMITATION OF ABSTRACT	18. NUMBER OF PAGES	19a. NAME OF RESPONSIBLE PERSON
a. REPORT	b. ABSTRACT	c. THIS PAGE			Carol Stoker
			UU	111	19b. TELEPHONE NUMBER *(Include area code)* (831) 656-3025

Mechanical Characterization of Lithium-Ion Battery Micro Components for Development of Homogenized and Multilayer Material Models

by

Kyle M. Miller

Submitted to the Department of Mechanical Engineering on May 10, 2014 in Partial Fulfillment of the requirements for the Degrees of

Naval Engineer
and
Masters of Science in Engineering and Management

Abstract

The overall battery research of the Impact and Crashworthiness Laboratory (ICL) at MIT has been focused on understanding the battery's mechanical properties so that individual battery cells and battery packs can be characterized during crash events.
The objective of this research is to better understand the battery component (electrode and separator) properties under different loading conditions. In this work, over 200 tests were conducted on battery components. These tests include uniaxial stress, biaxial punch, multilayer, single layer, short-circuit testing, wet vs dry specimen testing, strain rate testing, and more. Additionally, a scanning electron microscope was used to view the battery components at a micro level for the purpose of better understanding the aforementioned test results.
During these tests, it was observed that many of the electrodes in the Li-ion batteries are damaged during the battery manufacturing process. Also, the two methods of manufacturing battery separator were analyzed and their resulting mechanical properties were characterized.
These results will be used to further refine and validate a high-level, robust, and accurate computational tool to predict strength, energy absorption, and the onset of electric short circuit of batteries under real-world crash loading situations. The cell deformation models will then be applied to the battery stack and beyond, thereby enabling rationalization of greater optimization of the battery pack/vehicle combination with respect to tolerance of battery crush intrusion behavior. Besides improving crash performance, the finite element models contribute substantially to the reduction of the cost of prototyping and shorten the development cycle of new electric vehicles.

Thesis Supervisor: Tomasz Wierzbicki
Title: Professor of Structural Mechanics

(This Page is Intentionally Left Blank)

Acknowledgements

This thesis would not have been possible without the guidance and support of so many individuals who helped me achieve its completion. As such, I would like to express his sincere appreciation to the following:

- Honour Miller for her love and support. Without her, both this work and I would have been a jumbled mess.

- Dr. Tomasz Wierzbicki for his superb guidance and endless motivation during the entire year and a half that I have worked for him.

- Dr. Elham Sahraei for her keen eye at interpreting test results and for her guidance in leading the battery consortium at the ICL.

- CAPT Mark Thomas and CDR Jerod Ketcham for helping me to stay on track with both my future career and my current studies while at MIT.

- All members of the ICL, past and present, for helping to further the work on this project to the point that this thesis was possible.

- Mark and Jodie Miller for teaching me how to head confidently into the unknown.

- Chase Miller for reminding me what is really important.

Table of Contents

ACKNOWLEDGEMENTS **5**

TABLE OF CONTENTS **6**

TABLE OF FIGURES **8**

LIST OF TABLES **10**

1.0 INTRODUCTION **11**

2.0 BACKGROUND **11**

2.1 Review of Previous ICL Battery Research **11**

2.2 Goals of Current ICL Battery Research **12**

3.0 TESTING PROCEDURE AND RESULTS **12**

3.1 Lithium Ion Battery Specimen Type Overview **12**

3.2 Battery Component Uniaxial Tensile Tests **12**
3.2.1 Uniaxial Tensile Testing Procedure 13
3.2.2 Uniaxial Single Layer Tests 15
3.2.3 Uniaxial Strain Rate Effects on Separator Material 22
3.2.4 Uniaxial Multilayer Tests 25

3.3 Battery Component Biaxial Punch Tests **26**
3.3.1 Biaxial Testing Procedure 27
3.3.2 Possible Biaxial Testing Errors 28
3.3.3 Biaxial Single Layer Tests 30
3.3.4 Biaxial Multilayer Tests 33
3.3.5 Biaxial Punch Tests with Short Circuit Detection 35
3.3.6 Biaxial Multilayer Wet vs. Dry Tests 41

3.4 Micro-Mechanical Observations through Electron Microscopy **43**
3.4.1 Picture Orientation Nomenclature 43
3.4.2 Type A Battery SEM 44
3.4.3 Type B Material 50
3.4.4 Manufacturing Defects Viewed with SEM 53
3.4.5 Partially Damaged Specimens 54

4.0 CONCLUSIONS **57**

5.0 FUTURE WORK.....58

APPENDIX A LIST OF ACRONYMS AND ABBREVIATIONS 59

REFERENCES 60

Table of Figures

Figure 1 ICL Instron 5944 with Uniaxial Tension Grips 13
Figure 2 Uniaxial Testing Dogbone Specimen Specifications 14
Figure 3 Digital Image Correlation (DIC) Photo of Separator (Meier 2013) 15
Figure 4 Force vs Displacement Al Cathode (MD) 16
Figure 5 Force vs Displacement Al Cathode (TD) 16
Figure 6 Stress vs Strain Al Cathode (MD) 17
Figure 7 Stress vs Strain Al Cathode (TD) 17
Figure 8 Force vs Displacement Cu Anode (MD) 18
Figure 9 Force vs Displacement Cu Anode (TD) 18
Figure 10 Stress vs Strain Cu Anode (MD) 19
Figure 11 Stress vs Strain Cu Anode (TD) 19
Figure 12 Force vs Displacement Separator (MD) 20
Figure 13 Force vs Displacement Separator (TD) 21
Figure 14 Stress vs Strain Separator (MD) 22
Figure 15 Stress vs Strain Separator (TD) 22
Figure 16 Force vs Displacement Separator (MD) Variable Strain Rates 23
Figure 17 Force vs Displacement Separator (TD) Variable Strain Rates 23
Figure 18 Stress vs Strain Separator (MD) Variable Strain Rates 24
Figure 19 Stress vs Strain Separator (MD) Variable Strain Rates 24
Figure 20 Multilayer Test Specimen Layout 25
Figure 21 Force vs Displacement 4 Layer (MD) 26
Figure 22 Force vs Displacement 4 Layer (TD) 26
Figure 23 Biaxial Testing Mount 27
Figure 24 Instron 5944 Machine with Biaxial Punch Setup 27
Figure 25 Biaxial Testing Error 1 28
Figure 26 Specimen that was Over Tightened (left) and Specimen Undergoing Normal Failure (right) 29
Figure 27 Biaxial Testing Error 2 29
Figure 28 Specimen Experiencing Slippage (left) and Specimen Undergoing Normal Deformation (right) 30
Figure 29 Force vs Punch Travel Al Cathode Type A 30
Figure 30 Force vs Punch Travel Al Cathode Type B 31
Figure 31 Force vs Punch Travel Cu Anode Type A 31
Figure 32 Force vs Punch Travel Cu Anode Type B 32
Figure 33 Force vs Punch Travel Separator Type A (For zoomed view see Figure 35) . 32
Figure 34 Force vs Punch Travel Separator Type B 33
Figure 35 Type A Separator Small Cracks Development 33
Figure 36 Load vs. Punch Travel 3 Layer Type B 34
Figure 37 Summed Individual vs 3 Layer Biaxial Punch Tests Type B 34
Figure 38 Separator Material Provides Electrical Insulation 35
Figure 39 Anode Shows Conductivity to Electricity 36
Figure 40 Cathode Shows Non-conductivity to Electricity 36
Figure 41 Biaxial Punch Test Specimen Templates 37

Figure 42 Biaxial Punch Test Specimen Templates in Stacked Position 37
Figure 43 Biaxial Punch Test Specimen Templates in Stacked Position (Top View)..... 37
Figure 44 Separator Specimens Being Laser Cut 38
Figure 45 Biaxial Punch Test with Multi-meter 39
Figure 46 Test 461 Load vs Displacement 39
Figure 47 Test 462 Load vs Displacement 40
Figure 48 Test 463 Load vs Displacement 40
Figure 49 Test 464 Load vs Displacement 41
Figure 50 Force vs Punch Travel 4 Layer Type B- Wet..... 42
Figure 51 Force vs Punch Travel 4 Layer Type B- Dry 42
Figure 52 Battery Component 3D Representation..... 43
Figure 53 Battery Component Side View..... 44
Figure 54 Battery Component Top View..... 44
Figure 55 Uncoated Al Side View..... 45
Figure 56 Uncoated Aluminum Top View 45
Figure 57 Uncoated Copper Side View 46
Figure 58 Uncoated Copper Top View..... 46
Figure 59 Coated Aluminum Side View..... 47
Figure 60 Coated Aluminum Side View..... 47
Figure 61 Coated Aluminum Top View 47
Figure 62 Coated Aluminum Top view (corner) 48
Figure 63 Coated Copper Side View 48
Figure 64 Coated Copper Top View..... 49
Figure 65 Coated Copper Top View (Corner) 49
Figure 66 Separator Side View..... 50
Figure 67 Separator Side View..... 50
Figure 68 Coated Aluminum Top View 51
Figure 69 Coated Aluminum Top View (Corner)..... 51
Figure 70 Coated Copper Side View (Zoomed in on Right))..... 52
Figure 71 Coated Copper Top View..... 52
Figure 72 Separator Side View..... 53
Figure 73 Separator Side View..... 53
Figure 74 Bare Aluminum (Left) and Previously Coated Aluminum (Right)..... 54
Figure 75 Al Cathode at 1/4 (Top Left), 1/2 (Top Right), 3/4 (Bottom Left), and Full (Bottom Right) Breaking Displacements..... 55
Figure 76 Cu Anode at 1/4 (Top Left), 1/2 (Top Right), 3/4 (Bottom Left), and Full (Bottom Right) Breaking Displacements..... 56
Figure 77 Separator Material at 1/4 (Top Left), 1/2 (Top Right), 3/4 (Bottom Left), and Full (Bottom Right) Breaking Displacements 57

List of Tables

Table 1 Legend for CAD Renderings 37

1.0 Introduction

Recent developments in lithium-ion battery technology are enabling the rapid expansion of the electric car market. Still, barriers remain before electric cars can be brought to mass production. The most important of these obstacles are related to cost, weight, and safety. Most of the current research and developments deal with controlling the environment surrounding the battery. These efforts look at controlling the voltage discharge rate of the battery by using electronic controls, cooling the area around the battery to prevent overheating, and adding a large metal case to protect the battery from foreign object intrusion. The research of the Impact and Crashworthiness Laboratory (ICL) at MIT focuses on understanding the battery's mechanical properties so that individual battery cells and battery packs can be characterized during crash events (Wierzbicki and Sahraei 2013).
The objective of this research is to better understand the battery component (electrode and separator) properties under different loading conditions so that high-level, robust, and accurate computational tools can be developed in order to predict strength, energy absorption, and the onset of electric short circuit of batteries under real-world crash loading situations. These cell deformation models will then be applied to the battery stack and beyond, thereby enabling rationalization of greater optimization of the battery pack/vehicle combination with respect to tolerance of battery crush intrusion behavior.

2.0 Background

This work on Li-ion batteries is not the first to come out of the ICL, nor will it be the last. The following sections describe the previous work that has done at the ICL on batteries, as well as the goals of the current research.

2.1 Review of Previous ICL Battery Research

The ICL started research on Li-ion batteries in 2010 and is expected to continue until at least 2016. The work first started when it was realized that Li-ion battery manufacturers were using the design-build-test method for developing their technology, while most other areas of manufacturing were moving on to the finite element modelling method. The benefits of using a finite element model method for the development of Li-ion batteries included the cost savings, environmental saving, and time savings (Hill 2011).

In the first years, a representative volume element (RVE) of a Li-ion battery was developed by using testing results conducted on multiple small prismatic and pouch cells. The RVE model treated the battery as a homogenized solid rather than multiple layers of cathode, anode, and separator in order to reduce the computing power needed to run a simulation of the model. Initial results between the RVE model and physical test results showed good correlation (Sahraei, Hill and Wierzbicki 2010).

In the subsequent years, the RVE model was further refined by conducting lateral compression, and three point bending for cylindrical cells and indentation tests for

prismatic pouch cells. From these tests, the model was then made robust enough to be able to predict the point of short circuit following impact or indentation (Campbell 2012).

In the third year, further indentation tests were conducted on prismatic pouch cells. The third year tests studied the effects of changing the indenter shape as well as varying the battery's state of charge. Additionally, the third year of research led to the development of an initial testing program on the individual battery component layers (Meier 2013).

2.2 Goals of Current ICL Battery Research

The goals of the current research in the ICL deal with the further development and execution of an individual battery component testing program along with concurrent refinement of the FEM at the battery component, cell, module, and pack levels. On January 1st 2014 the ICL began a 3 year research project with partners from industry in which the main deliverable from the ICL will be a calibrated and validated computational model in LS-Dyna and/or ABAQUS commercial software. These models will allow industry partners to optimize their individual battery designs and protective structures for maximized mechanical integrity against short circuit due to impact (Wierzbicki and Sahraei 2013).

3.0 Testing Procedure and Results

Testing on components from two different types of Li-ion batteries were conducted in this work. The following sections describe the equipment, preparation, and results from those tests. After the battery component descriptions, the uniaxial tension tests results are described first, followed by the biaxial punch tests, and finally the scanning electron microscope (SEM) results.

3.1 Lithium Ion Battery Specimen Type Overview

When put under extreme loading conditions, lithium ion batteries tend to exhibit large energy discharges which can result in fire and the rapid release of toxic gases (Meier 2013). This energy discharge event is shocking to behold and, could be easily used to damage a battery manufacturer's reputation if taken out of context. Therefore, the battery manufactures that have donated their battery material to the ICL have asked to remain anonymous. As such, the two brands of batteries used for testing in this study will be referred to as battery type A and battery type B.

Both types of battery components were obtained by the ICL in their dry, electrolyte-free state in order to prevent the discharge of any toxic gases that are usually associated with the burning of electrolyte. Most of the tests in this study were done on components in their dry state, but the differences in mechanical properties of battery components in their wet versus dry states is investigated in Section 3.3.6

3.2 Battery Component Uniaxial Tensile Tests

Uniaxial tensile tests were conducted on type B battery only. The uniaxial tests conducted on battery type A were completed in previous work (Meier 2013).

First, testing was completed on each single layer of battery component. This test was done both in the machine and transverse direction of the component. Second, multilayer tests consisting of two separator, one anode, and one cathode components was conducted to better understand the interactions between layers. The multilayer test was also completed in the machine and transverse direction. Finally, variable displacement rate speeds were used on the separator material in order to quantify the effects of strain rate.

3.2.1 Uniaxial Tensile Testing Procedure

The uniaxial tensile battery component testing conducted at the ICL was completed using the Instron Test Machine Model 5944, shown in Figure 1. For uniaxial testing purposes, the machine is outfitted with a 100N load cell and two 2kN pneumatic grips. The grips were fitted with a 25x32mm rubber face that was able to properly secure the battery component specimens without slipping or ripping.

Figure 1 ICL Instron 5944 with Uniaxial Tension Grips

From previous work on uniaxial tensile testing of battery components, it was found that the best specimen preparation procedure was to use a dogbone specimen with a parallel length (Lp) of 10 template made out of 1.5 mm aluminum sheet (Meier 2013). The specifications of this template are shown in Figure 2.

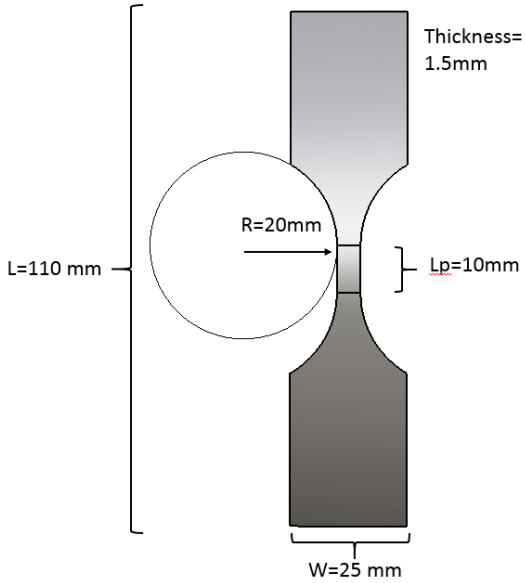

Figure 2 Uniaxial Testing Dogbone Specimen Specifications

Once the template was made from a waterjet cutting machine, precisely dimensioned battery component specimens could be rapidly created by using an X-ACTO knife. These specimens were then carefully placed into the pneumatic grips of the Instron machine and lightly tensioned to approximately 0.3 N for testing.

The Bluehill®3 software package that was included with the Instron machine is used to measure the force seen by the pneumatic grips as well as the overall displacement during testing. The stress of the specimens could be calculated by dividing the force seen by the grips by the cross sectional area of the parallel midbody section of the dog bone.

To calculate the strain seen within the specimen, a digital image correlation (DIC) software package called Vic-Snap® and Vic-2D® was used. This software requires the dog bone specimens to be first lightly speckled with a spray paint solution before being placed in the testing machine. An Imaging Retiga 1300i digital camera was used to take photographs of the specimen at one second intervals as it was pulled apart by the pneumatic grips. The software internally tracks the distance between the speckled dots of the spray paint and can determine the strain seen at every location on the specimen. Figure 3 shows an example of how the software tracks the strain within a specimen of battery separator material.

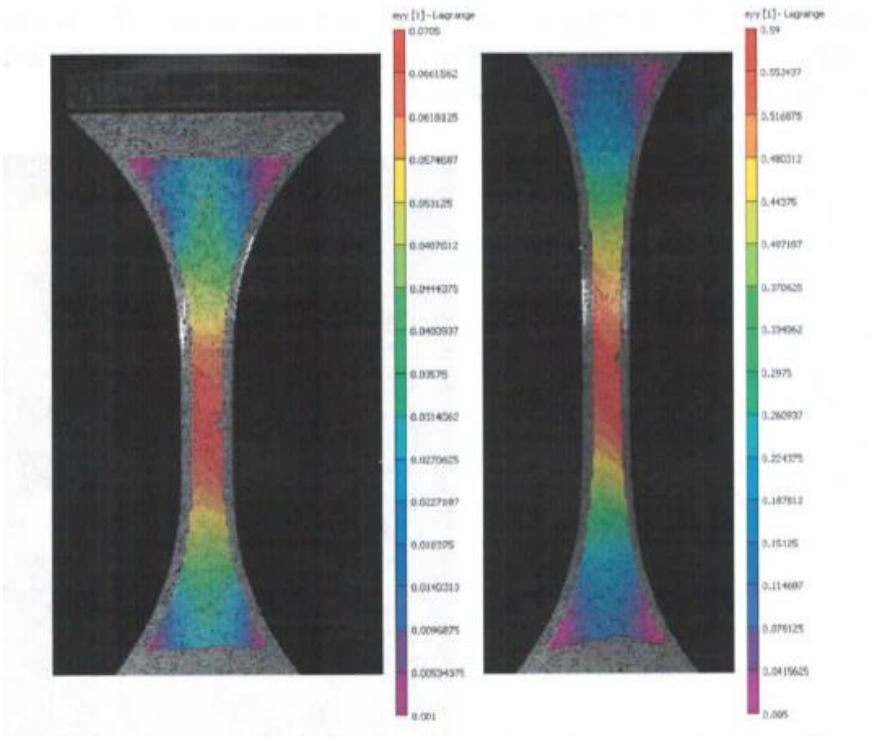

Figure 3 Digital Image Correlation (DIC) Photo of Separator (Meier 2013)

The stress and strain obtained from the two different methods mentioned above could then be combined onto one graph for material property characterization.

3.2.2 Uniaxial Single Layer Tests

3.2.2.1 Aluminum Cathode

After ten aluminum cathode specimens were prepared for uniaxial tension testing as described in section 3.2.1, uniaxial tension tests were conducted in both the machine and transverse directions of battery type B. These tests were conducted in order to ensure repeatability of the testing method, as well as to acquire data for production of a stress/strain curve. All of the tests were conducted at a cross head speed of 0.2 mm/min. The results of the tests in the machine direction are shown in Figure 4 and the transverse direction results are shown in Figure 5.

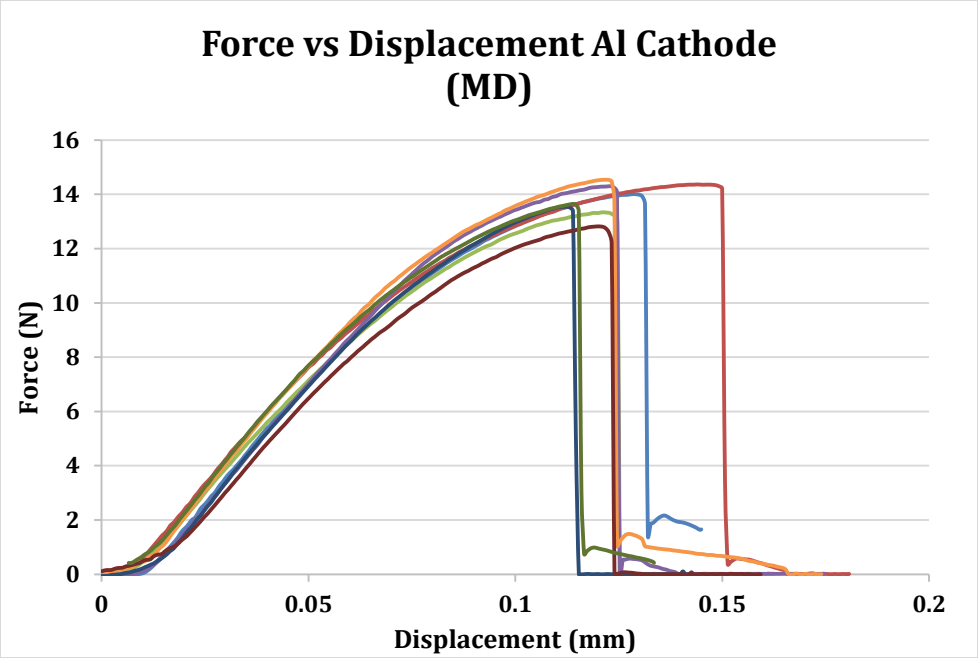

Figure 4 Force vs Displacement Al Cathode (MD)

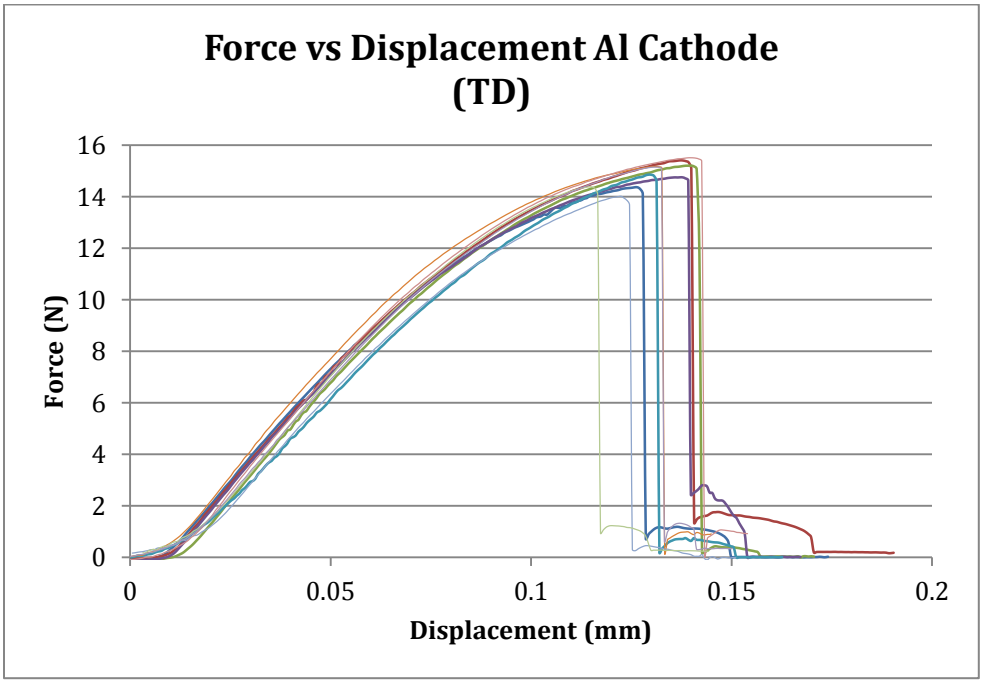

Figure 5 Force vs Displacement Al Cathode (TD)

As seen in the above figures, the breaking strength of the Al cathode is almost the same in the transverse and machine direction. In both directions the specimens break at a force of 15 N and displacements of 0.13-0.15 mm. The tests showed good repeatability throughout the different specimens in both the transverse and machine directions.

Next a representative specimen was chosen from each set of tests for the development of a stress/strain curve. DIC data was processed as described in section 3.2.1 to acquire the strain of the material, and the cross section of the specimen was measured to acquire the stress seen within the material. The stress and strain for each direction of testing were then placed on a single graph as shown Figure 6 and Figure 7.

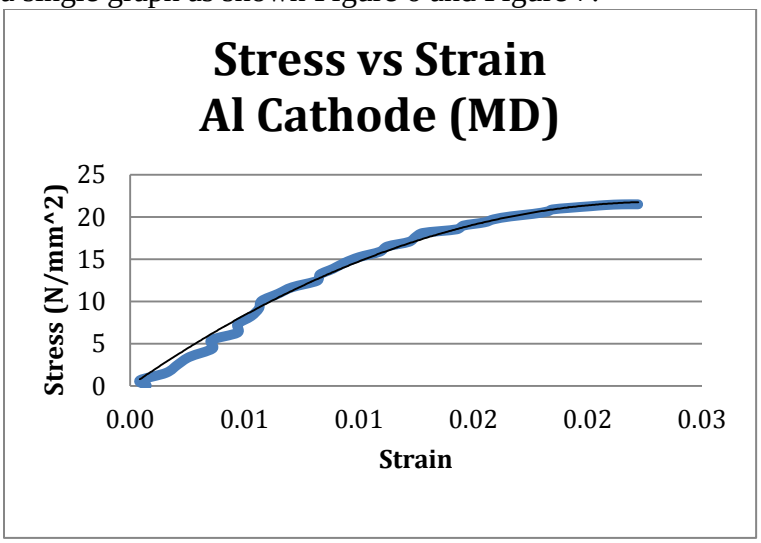

Figure 6 Stress vs Strain Al Cathode (MD)

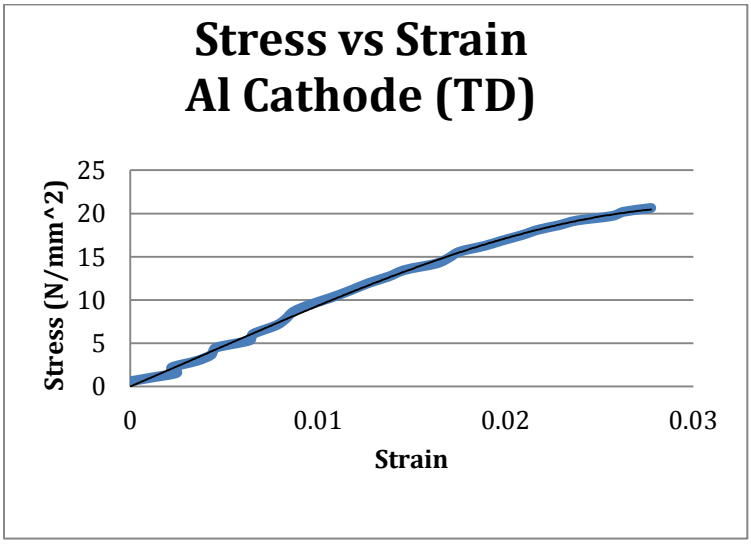

Figure 7 Stress vs Strain Al Cathode (TD)

As seen in the above figures, there was quite a bit of noise in the DIC processing of these tests. The author believes this to be due to the fact that the coating of the cathode was not moving in the same manner as the underlying aluminum foil during the testing. The author also noticed that the $LiCoO_2$ coating of the aluminum foil was much easier to remove from the aluminum foil than the carbon coating of the copper foil. This could also play into the noise factor of the DIC. However, the general shape of the stress strain curve could still be determined from these tests and will be used in future work for the validation of a FEM for the Al cathode.

3.2.2.2 Copper Anode

Next ten copper anode specimens were prepared for uniaxial tension testing as described in section 3.2.1, uniaxial tension tests were conducted in both the machine and transverse directions of battery type B. As with the Al cathode, this many tests were needed in order to ensure repeatability of the testing method, as well as to acquire data for the development of a stress/strain curve for the copper anode. To ensure comparability with the Al cathode tests, the Cu anode tests were also conducted at 0.2 mm/min. The results of the tests in the machine direction are shown in Figure 8 and the transverse direction results are shown in Figure 9.

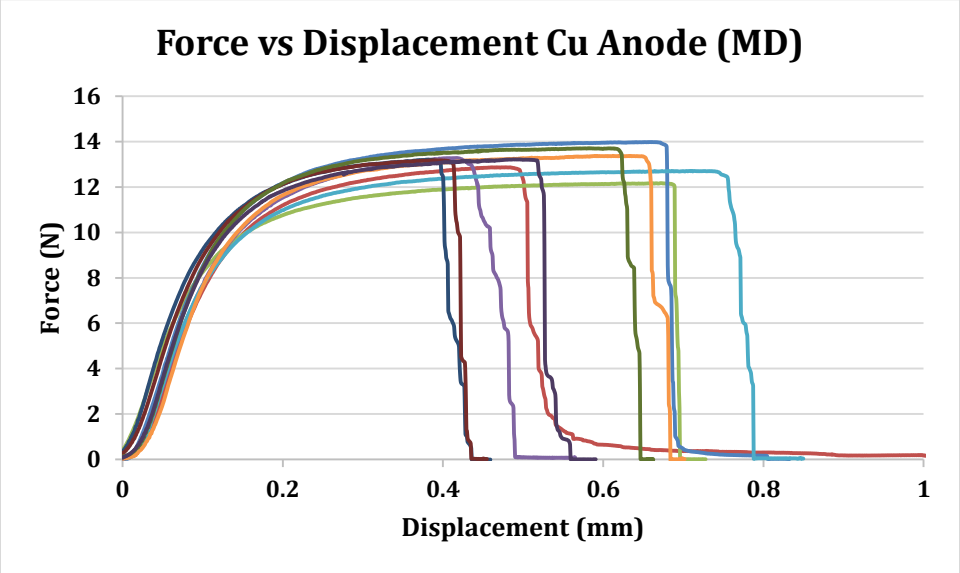

Figure 8 Force vs Displacement Cu Anode (MD)

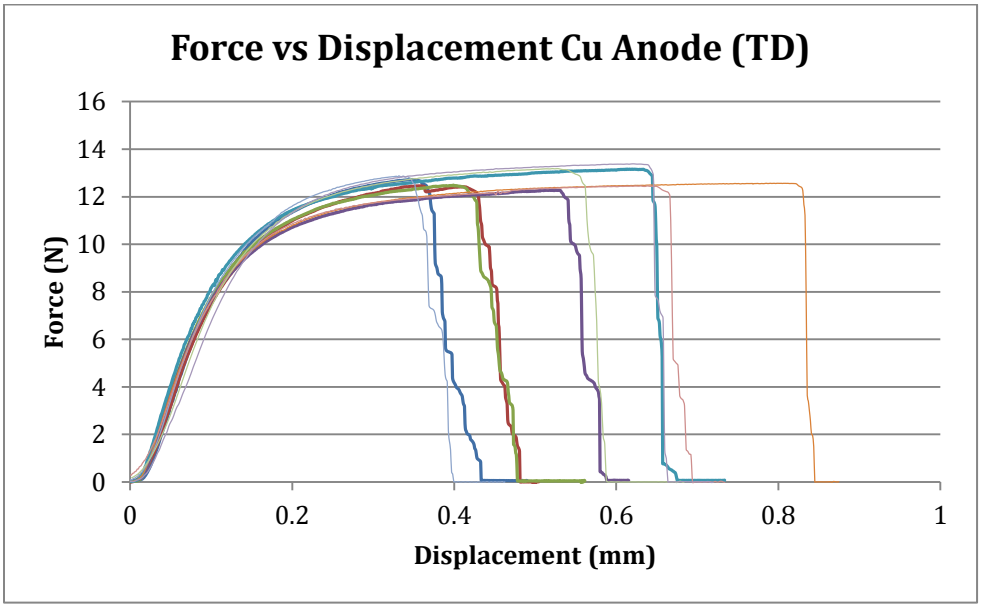

Figure 9 Force vs Displacement Cu Anode (TD)

As seen in the above figures, the Cu anode has similar breaking strength and displacement in both the machine and transverse direction. It also has a slightly lower breaking strength than the Al cathode, but its breaking displacement is almost 6 times higher. Also of note from these tests is that the variability in breaking displacement is higher than with the Al cathode. Further discussion on the increased breaking displacement variability of the Cu anode is located in section 3.4 of this report.

After the Cu anode uniaxial tension tests were completed, a representative specimen was chosen from each set of tests for the development of a stress/strain curve. The DIC data that was collected during the test was processed as described in section 3.2.1 to acquire the strain of the material, and the cross section of the specimen was measured to acquire the stress seen within the material. The stress and strain for each direction of testing were then placed on a single graph as shown Figure 6 and Figure 7.

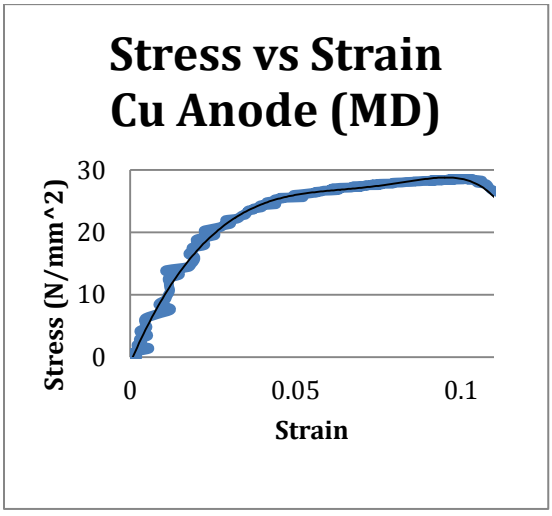

Figure 10 Stress vs Strain Cu Anode (MD)

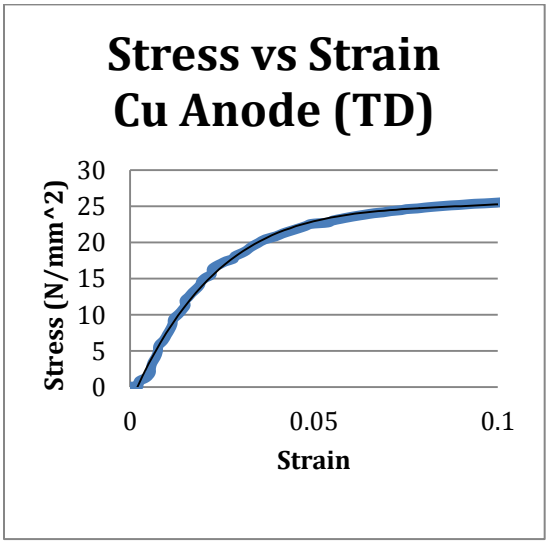

Figure 11 Stress vs Strain Cu Anode (TD)

As seen in the above figures, there was some noise associated with the DIC image processing of these tests, especially in the MD. The author believes this to be due to the fact that the coating of the cathode was not moving in the same manner as the underlying copper foil during the testing. However, the general shape of the stress strain curve could still be determined from these tests and will be used in future work for the validation of a FEM for the Cu anode.

3.2.2.3 Separator

For the type B separator material uniaxial tension tests, specimens were prepared as described in section 3.2.1. Ten uniaxial tension tests were conducted in both the machine and transverse directions. Previous research on uniaxial tension tests of type A battery separator led the author to believe that the type B separator would be highly anisotropic (Meier 2013). However, as seen in Figure 12 and Figure 13, the separator material of battery type B is much less anisotropic than type A separator was shown to be.

It should be noted here that the MD tests were conducted at 4 mm/min and the TD tests were conducted at 6 mm/min. The effects of varying the strain rate on this separator material are discussed in section 3.2.3, but the differences are such that the results from a tests conducted at 4 mm/min can be compared with the results from a test run at 6 mm/min with minimal error.

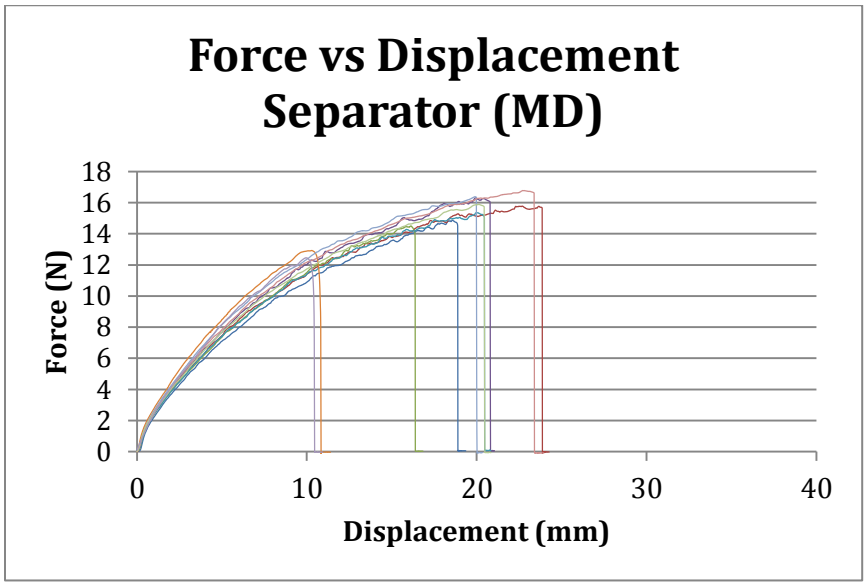

Figure 12 Force vs Displacement Separator (MD)

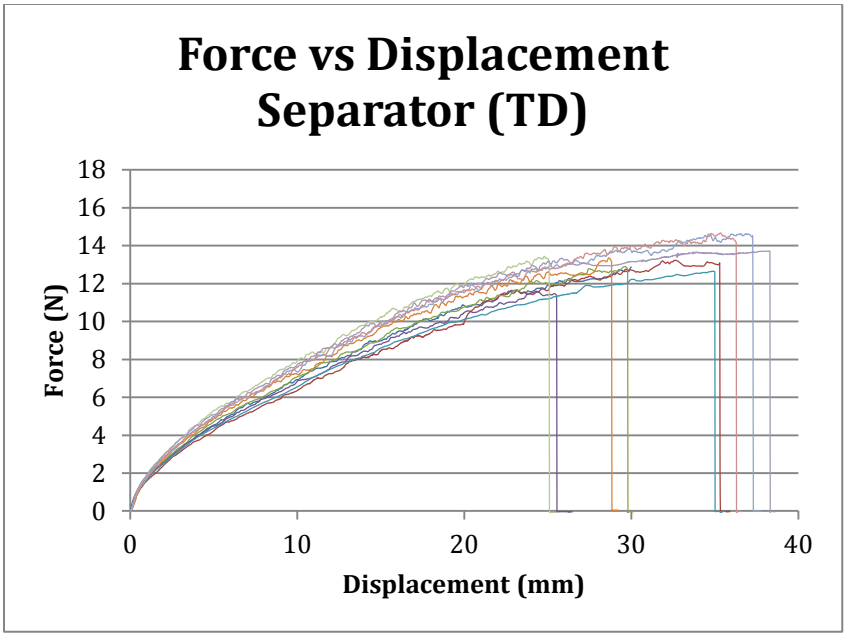

Figure 13 Force vs Displacement Separator (TD)

As seen in the above figures, this separator material is slightly anisotropic. The average breaking resistance seen by the Instron machine is 15 N in the MD and 13 N in the TD. The average breaking displacement for the separator was 19 mm in the MD and 33 mm in the TD. These results led the author to believe that the type B separator material was manufactured in a different method than the type A separator material.

Currently, Li-ion battery separator materials are manufactured by using either a wet or dry process (Jeon and Kim 2007). The wet process consists of mixing a polymer film with an additive and extruding it through a sheet die. The additives are then removed to allow for a porous structure (Gwon, Choi and Sohn 2009). The dry process consists of creating a sheet of polymer film and stretching it in one direction create small pores. This is known as the "crazing" process (Zhang, Ervin and Xu 2004).

The wet separator manufacturing process is known to allow for more charging cycles and better mechanical properties, while the dry manufacturing process is known to be able to produce a battery with a higher power density (Jeon and Kim 2007). From the uniaxial testing results shown above, the author hypothesized that the type A battery was manufactured using a dry process, while the type B battery was manufactured using a wet process. Further discussion on the types of manufacturing processes used in each type of battery separator can be read in section 3.4

After the separator uniaxial tension tests were completed, a representative specimen was chosen from each set of tests for the development of a stress/strain curve. The DIC data that was collected during the test was processed as described in section 3.2.1 to acquire the strain of the material and the cross section of the specimen was measured to acquire the stress seen within the material. The stress and strain for each direction of testing were then placed on a single graph as shown Figure 14 and Figure 15.

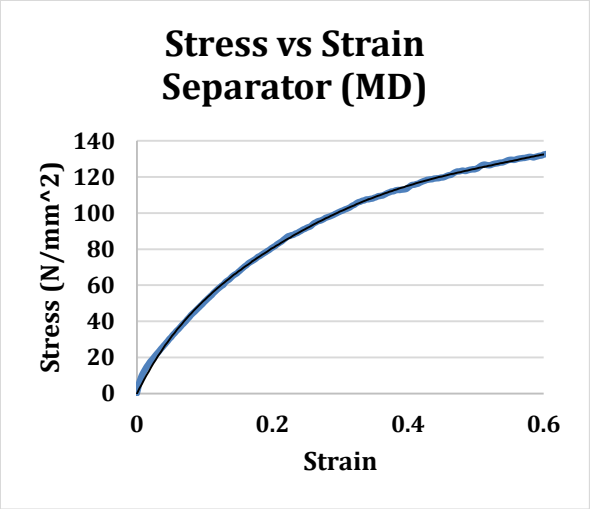

Figure 14 Stress vs Strain Separator (MD)

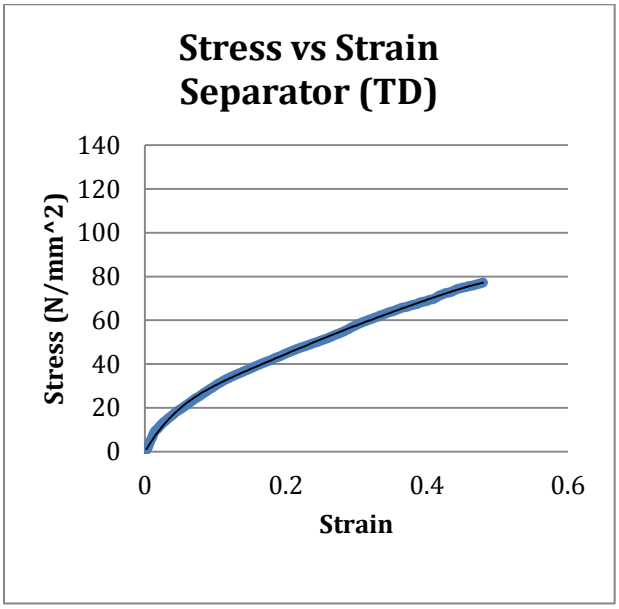

Figure 15 Stress vs Strain Separator (TD)

As seen in the above figures, there was less noise in the DIC data associated with the separator tests than with either the Cu anode or Al cathode. The only trouble that the author encountered during this section of the data processing was that the separator stretched so far during the test that it would sometimes move itself out from the field of view of the DIC camera. After a few iterations, the solution was found by widening the field of view of the camera so that it could capture the stretched separator specimen, but not too far as to blur the speckled dots of the spray paint on the specimen. These stress strain curves will be used in future work for the validation of the FEM for the separator.

3.2.3 Uniaxial Strain Rate Effects on Separator Material

The next step in the uniaxial component testing was to understand the effects of strain rate on the separator material. In this set of tests, multiple separator specimens

underwent uniaxial strain tests at speed from 4 mm/min to 1000 mm/min in both the MD and TD. In Figure 16 and Figure 17 a representative specimen from each testing speed was chosen and placed on the same force versus displacement plot.

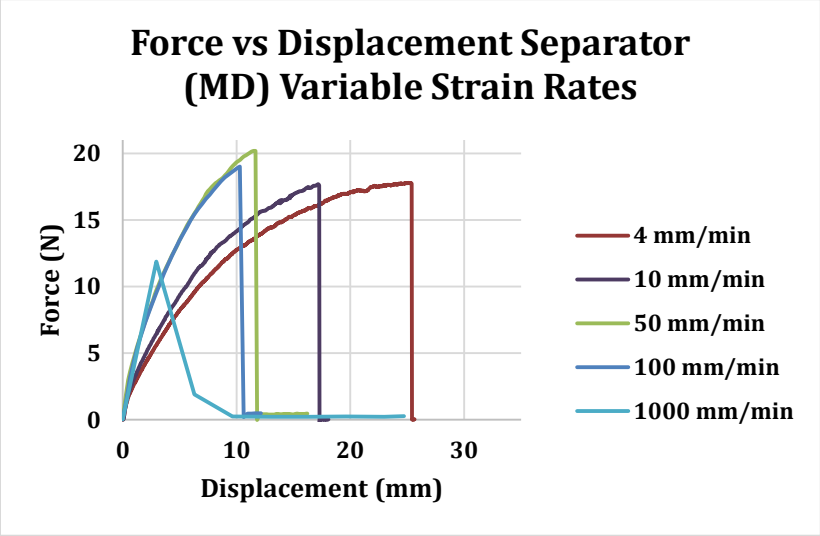

Figure 16 Force vs Displacement Separator (MD) Variable Strain Rates

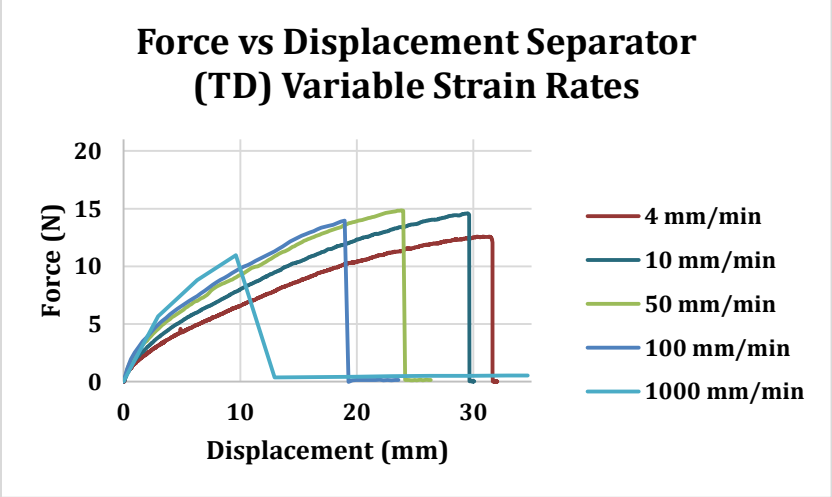

Figure 17 Force vs Displacement Separator (TD) Variable Strain Rates

As seen in the above figures, as the speed of the test increases, the breaking displacement of the separator drastically decreases. In the MD, the breaking displacement of the separator goes from 25 mm for the 4 mm/min test to only 4 mm for the 1000 mm/min test. In the TD, the breaking displacement goes from 32 mm for the 4 mm/min test to only 9 mm for the 1000 mm/min test. The breaking resistance force did not change significantly as the speed of the test changed in either the MD or TD. It should be noted here that the Bluehill® software measures the force and displacement of the test at 0.2 second intervals, therefore the breaking resistance and displacement of the 1000 mm/min test should not be used for anything other than to compare with the slower tests because the test traveled over 3 mm between measurements. This is also why the 1000 mm/min test curve does not appear as smooth as the slower tests.

After the separator uniaxial tension tests with variable strain rates were completed, a representative specimen was chosen from each set of tests for the development of a stress/strain curve. The DIC data that was collected during the test was processed as described in section 3.2.1 to acquire the strain of the material, and the cross section of the specimen was measured to acquire the stress seen within the material. The stress and strain for each direction of testing for the 4 mm/min and 10 mm/min tests were then placed on a single graph as shown in Figure 18 and Figure 19.

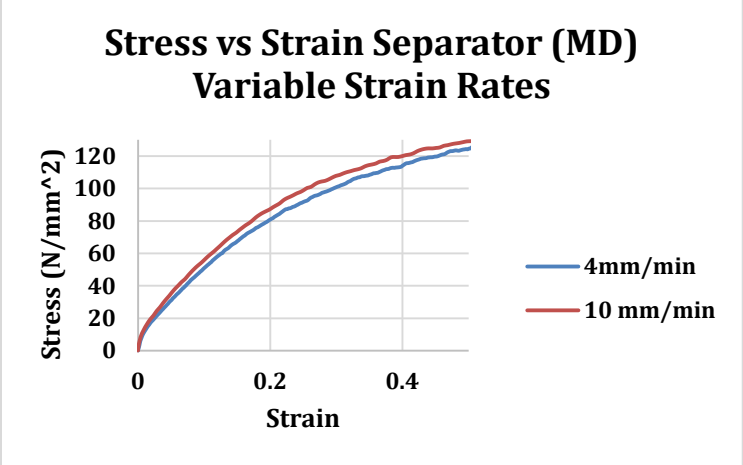

Figure 18 Stress vs Strain Separator (MD) Variable Strain Rates

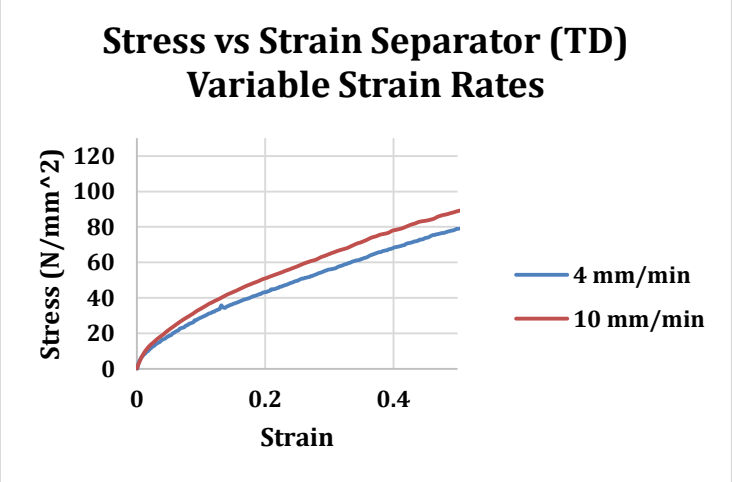

Figure 19 Stress vs Strain Separator (MD) Variable Strain Rates

As seen in the above figures, when the test is run at a faster rate, the stress for a given strain value is higher for the separator material. Further work in this area should focus on optimizing the exposure time of the camera for the speed of the test. The author believes that, during the faster tests the camera exposure time was too long, and therefore was unable to capture the exact location of the paint speckles. This made the DIC data for the faster tests unusable for this work. These stress strain curves will be used in future work for the further validation of the FEM separator material.

3.2.4 Uniaxial Multilayer Tests

The final type of uniaxial stress test conducted in this study involved stacking the anode, cathode and 2 layers of separator material as shown in Figure 20. The order of stacking was, from front to rear, Al cathode, separator, Cu anode, and separator. This test was conducted to help further refine the homogenized FEM that was developed in earlier studies. The tests were conducted at 5 mm/min in both the MD and TD, and the results are displayed in Figure 21 and Figure 22.

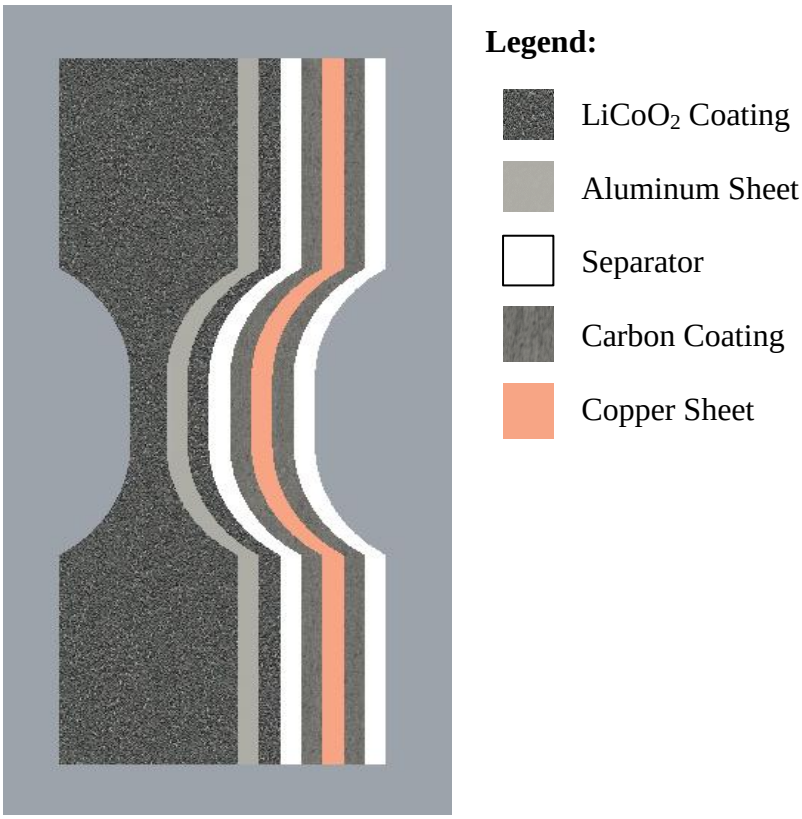

Figure 20 Multilayer Test Specimen Layout

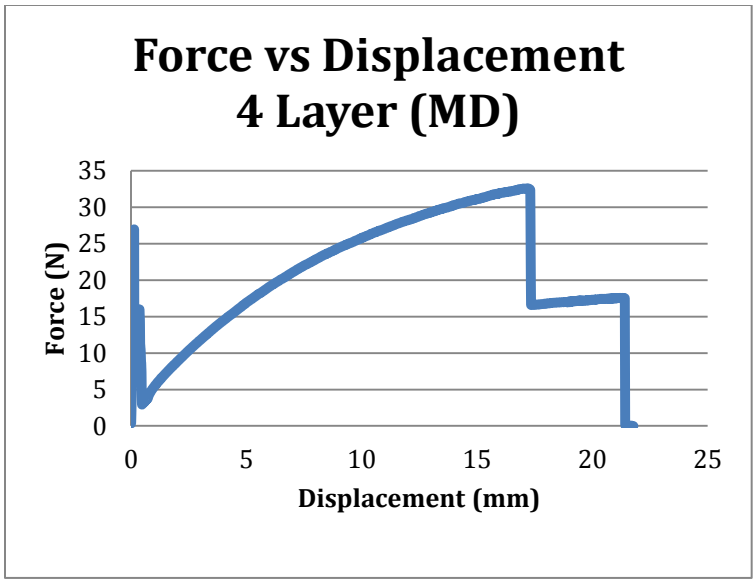

Figure 21 Force vs Displacement 4 Layer (MD)

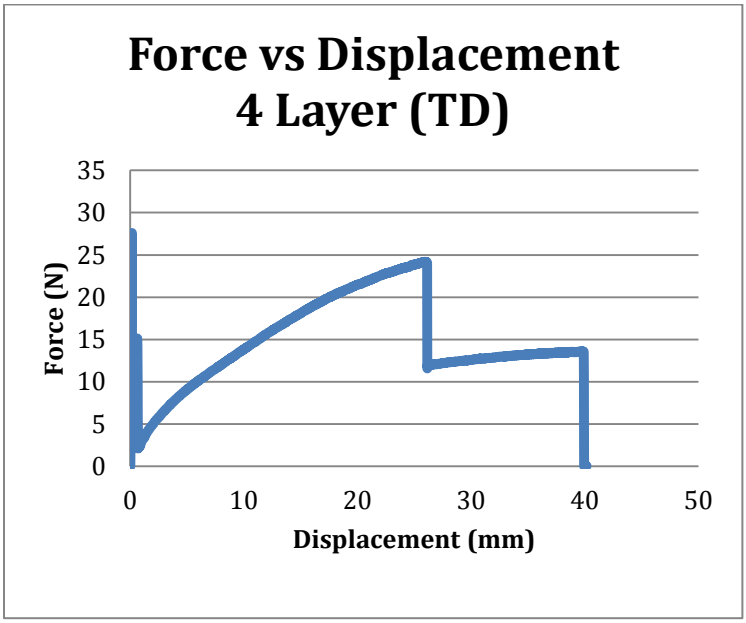

Figure 22 Force vs Displacement 4 Layer (TD)

As shown in the figures above, during the multilayer tests the Al cathode breaks first at 0.15 mm, followed by the Cu anode at 0.6 mm, and finally the 2 layers of separator break last. There seemed to be very little interaction between the layers during the test, and therefore the results of the multilayer tests are similar to what one would see if a summation of the individual component tests was plotted. These results will be used for further development of the homogenized FEM for Li-ion batteries at the ICL.

3.3 Battery Component Biaxial Punch Tests

To further understand the mechanical properties of each battery component, biaxial punch tests were conducted on batteries type A and B. The following sections describe

the procedure for biaxial punch testing of battery components, errors that may occur while testing, and the actual test results from this study.

3.3.1 Biaxial Testing Procedure

A mount was developed by Xiaowei Zhang of the ICL for biaxial punch testing of thin specimens with the Instron Test Machine Model 5944. I 3d model image of the mount is shown in Figure 23.

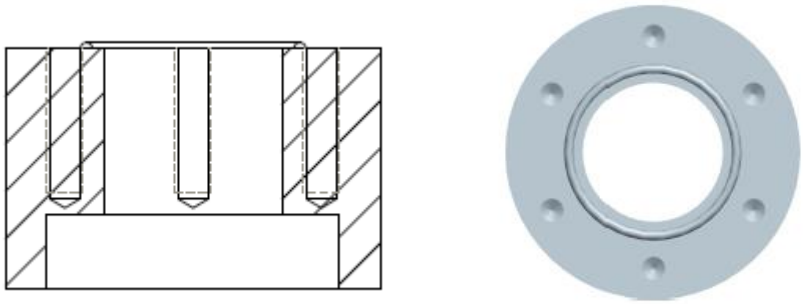

Figure 23 Biaxial Testing Mount

The mount made to be placed is a hollow box made out of steel with a 29 mm diameter hole in the top to allow for punch penetration through the specimen. A circular groove along the outside of the hole was designed specifically to help the mount to with specimen holding. Six machine drilled holes are equally spaced along the outside of the groove into which the mount head could be drilled into for securement of the specimens. A picture of the Instron test machine with the biaxial punch test mounting device installed is shown in Figure 24.

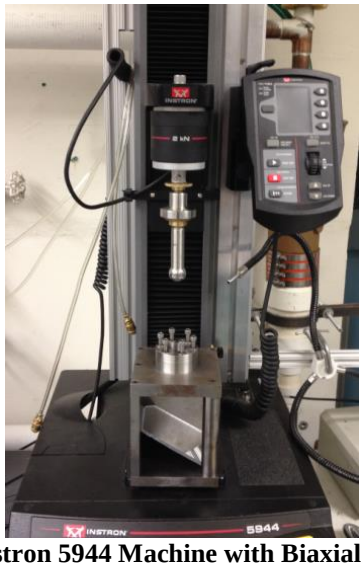

Figure 24 Instron 5944 Machine with Biaxial Punch Setup

For all biaxial tests conducted in this study a smooth spherical steel punch was used. The spherical punch had a radius of 25 mm.

As was the case in the uniaxial test specimens, the biaxial test specimens were cut out using an X-acto® knife. The cutting template was a circle of diameter 32 mm that was chosen so that the specimens would fit properly into the mount.

The six nuts located on the mount used for biaxial punch test were hand tightened using American Society of Mechanical Engineers (ASME) recommended tightening procedure (ASME 2001). After multiple tests, it was found that the proper tightening of these very thin battery component specimens was somewhat difficult. The results of either over tightening or under tightening the specimens are discussed in the following section.

3.3.2 Possible Biaxial Testing Errors

As mentioned in the previous section, the author encountered difficulties in the mounting procedure of the biaxial tests that were conducted in this work. The first difficulty was the error of over tightening of the specimen. As shown in Figure 25, over tightening the specimen resulted in a loss of the peak force resistance that is seen in specimens that are correctly tightened in the mount.

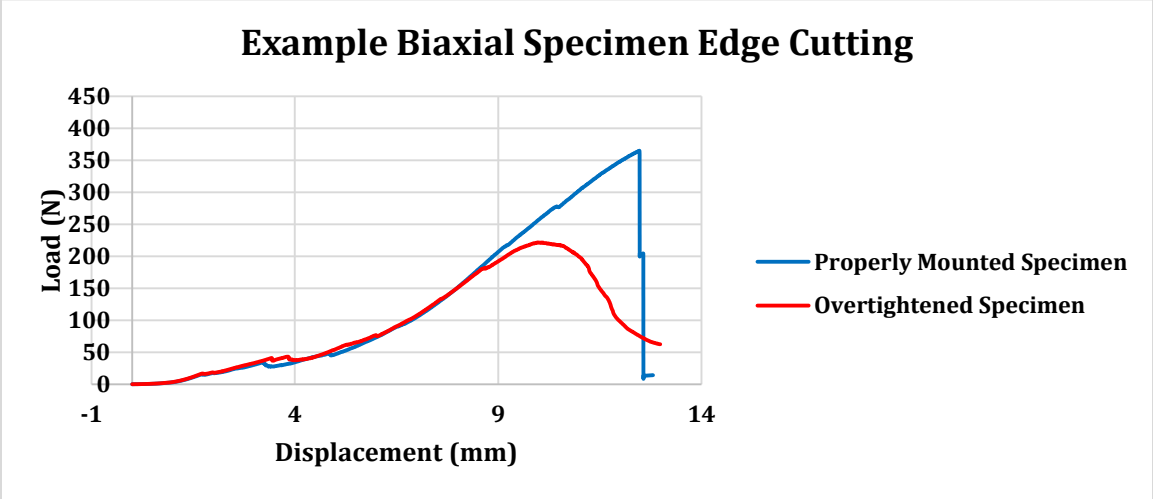

Figure 25 Biaxial Testing Error 1

This loss of peak force resistance due to over tightening can be explained by the associated rips found on the specimens along the edge of the mounting hole. As seen in Figure 26, an over tightened specimen begins ripping along the edge of the mounting hole and the ripping force observed by the Instron machine is nearly constant for a period of time.

Figure 26 Specimen that was Over Tightened (left) and Specimen Undergoing Normal Failure (right)

The second error that the author encountered during the mounting of biaxial punch testing was the issue of under tightening. As seen in Figure 27, under tightening of the specimen is associated with the sudden loss of force resistance to the punch. Unlike the over tightened specimen, here there is no gradual loss of force but rather an instant loss of force resistance by the specimen. This is followed by the return of the force resistance for a short period and then a final break of the specimen.

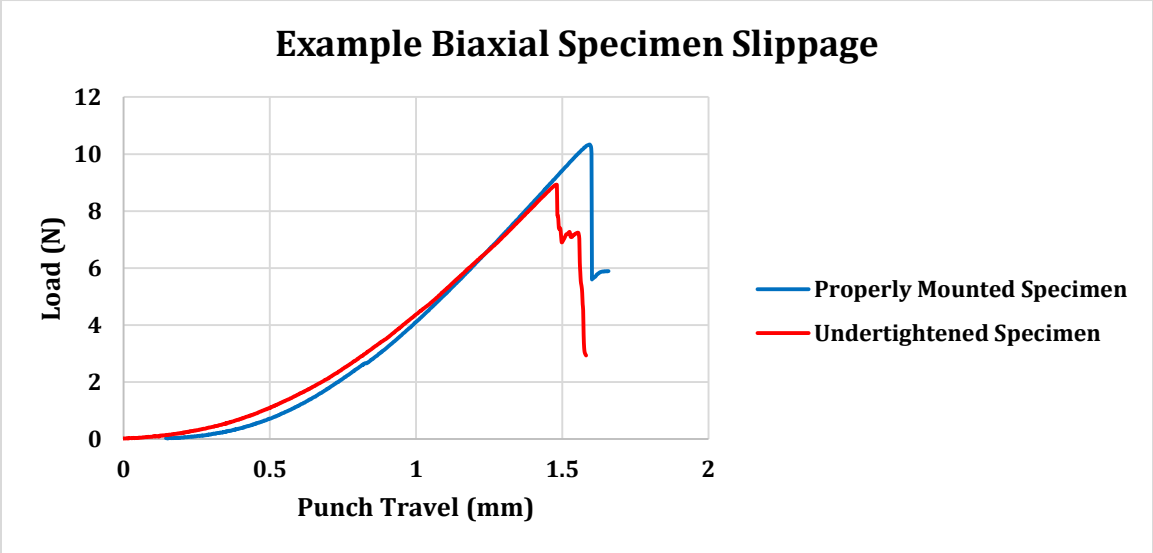

Figure 27 Biaxial Testing Error 2

In order to better understand what is physically happening in the under tightened specimen, photos were taken during the test. The photos show that when the under tightened specimen has been brought to its first loss of force resistance, the specimen slips from its mounting and wrinkles as shown in Figure 28. The author hypothesizes that once the wrinkles are formed, the effective thickness of the specimen in the mount thickens, thereby retightening the specimen and regaining its ability to resist the force of the punch. However, it is folded on top of itself and damaged, so is no longer able to hold the full load that is seen in the unfolded specimen.

Figure 28 Specimen Experiencing Slippage (left) and Specimen Undergoing Normal Deformation (right)

Once these testing errors were better understood by the author, he could then understand when his tests results were accurate or not. These errors were also noted so that other members of the ICL could better understand how to interpret their testing results if they didn't get the output they were expecting.

3.3.3 Biaxial Single Layer Tests

The biaxial testing began with each component type from batteries A and B. The results are presented below, and are organized such that the results from battery type A and then B are shown from a single component before moving on to the next component.

3.3.3.1 Al Cathode

The biaxial testing began with the Al cathode of battery types A and B. Five specimens were tested from each battery type in order to ensure repeatability of the testing procedure. Figure 29 and Figure 30 below display the force vs. punch travel for each of the battery types.

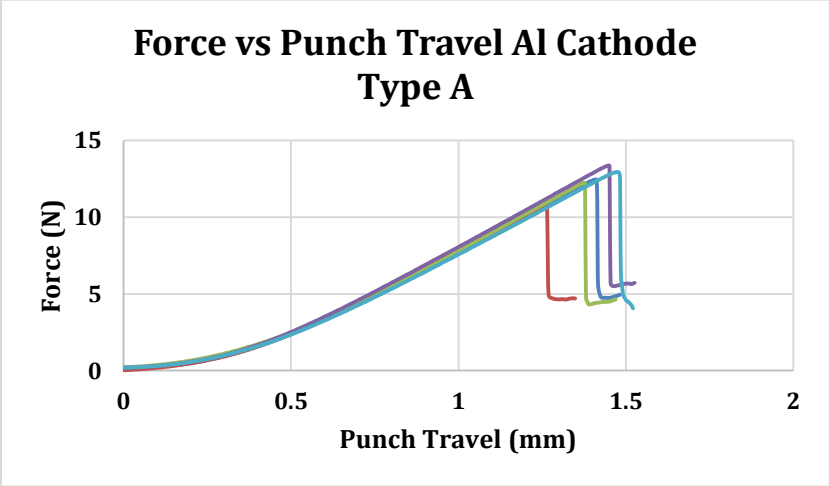

Figure 29 Force vs Punch Travel Al Cathode Type A

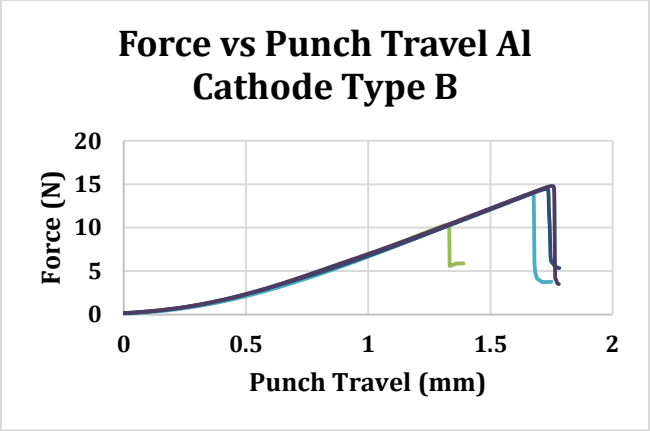

Figure 30 Force vs Punch Travel Al Cathode Type B

As seen in the above figures, the average Al cathode from battery type A breaks at 12.5 N and 1.4 mm while the Al cathode from battery type B breaks at 14 N and 1.6 mm. It should be noted that this small difference in breaking strength could be attributed to the fact that the type A cathode is slightly thinner than the type B, but there are too many unknowns in the manufacturing process of each type to directly attribute the increased strength to the increased thickness.

3.3.3.2 Cu Anode

Next, the Cu Anode from battery type A and B were testing in the biaxial punch fixture. Five specimens of each type were tested to ensure repeatability of the testing method for this material. Figure 31 and Figure 32 show the test results.

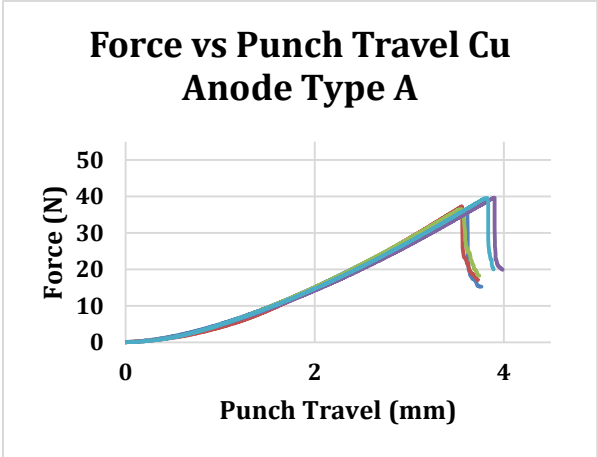

Figure 31 Force vs Punch Travel Cu Anode Type A

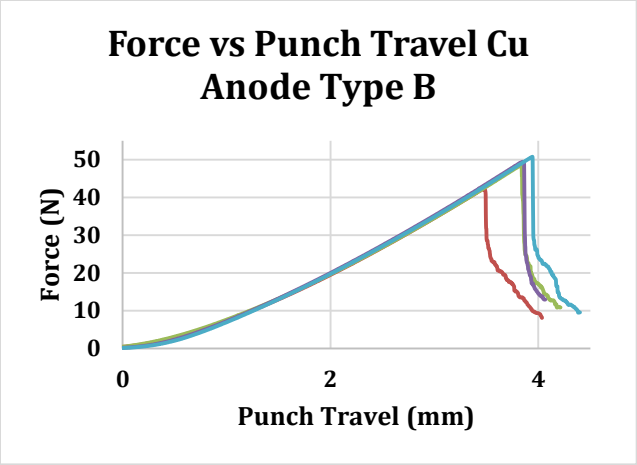

Figure 32 Force vs Punch Travel Cu Anode Type B

As seen in the above figures, the average distance of punch travel for the Cu Anode was 3.8 mm for both battery type A and B. Battery type A saw approximately 39 N of resistance before breaking while type B say 58 N. The Cu Anode of both types of batteries had a stronger breaking resistance and a longer punch travel before breaking than the Al cathode.

3.3.3.3 Separator

Next, the separator material from battery type A and B were testing in the biaxial punch fixture. Five specimens of each type were tested to ensure repeatability of the testing method for this material. Figure 33 and Figure 34 show the test results.

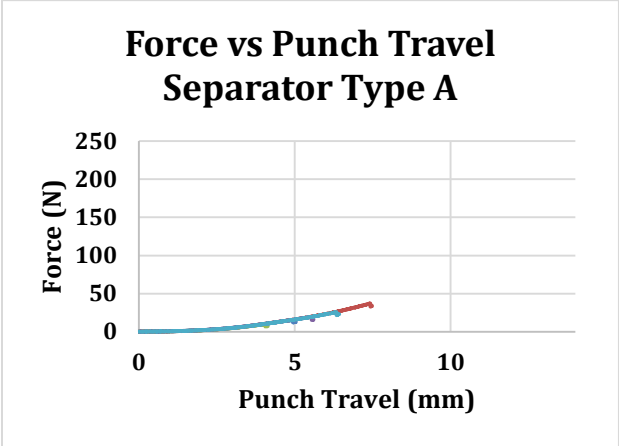

Figure 33 Force vs Punch Travel Separator Type A (For zoomed view see Figure 35)

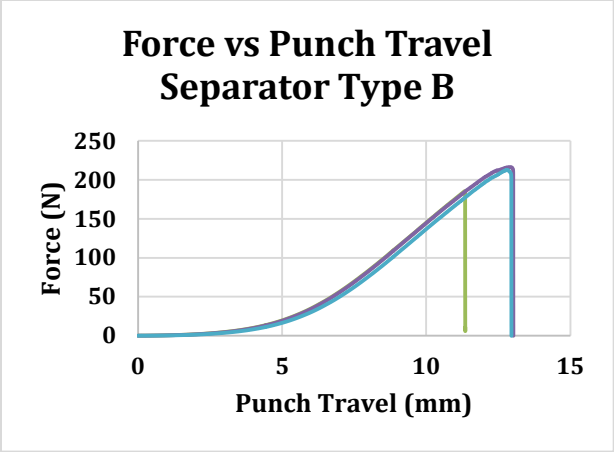

Figure 34 Force vs Punch Travel Separator Type B

As seen in the above figures, the average punch travel before breaking for the separator material was 6 mm for battery type A and 12 mm for battery type B. The average breaking resistance was 22 N for battery type A and 200 N for type B. The separator material of both types of batteries breaks, on average, after the punch has traveled further than the Cu Anode or Al Cathode.

The uniaxial tests showed that the separator material from the type A battery is highly anisotropic, as it was shown to provide very little resistance to strain in the TD. These biaxial tests provide two interesting results in regard to the previous findings. The first is that, in all of the tests, after the punch had traveled over 5mm, the specimen either broke or developed small cracks as shown in Figure 35. The second interesting finding was that all of the cracks that developed were along the MD. This reinforces the idea that the material is very weak in the TD.

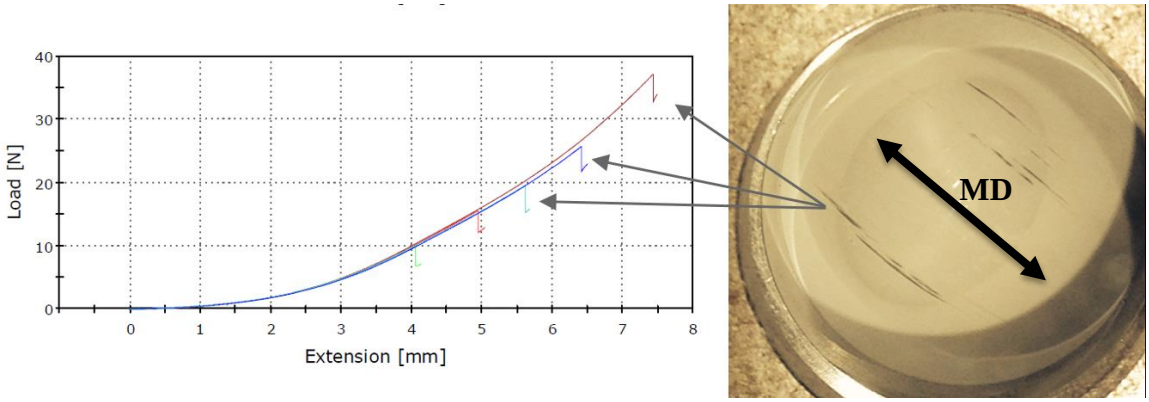

Figure 35 Type A Separator Small Cracks Development

3.3.4 Biaxial Multilayer Tests

Next, the individual components from battery type B was layered on top of each other as it would be in a battery and put through the same type of biaxial punch testing as in the previous section. The layers were, from top to bottom, Al cathode, separator, and Cu

anode. This experiment was repeated 5 times to ensure repeatability of the testing method.

The goal of this type of experiment was to see if we could better understand how a battery fails by monitoring the load and displacement of the multilayer specimen throughout a biaxial punch test. The results of the test are shown in Figure 36, along with arrows indicating the failure of each type of component.

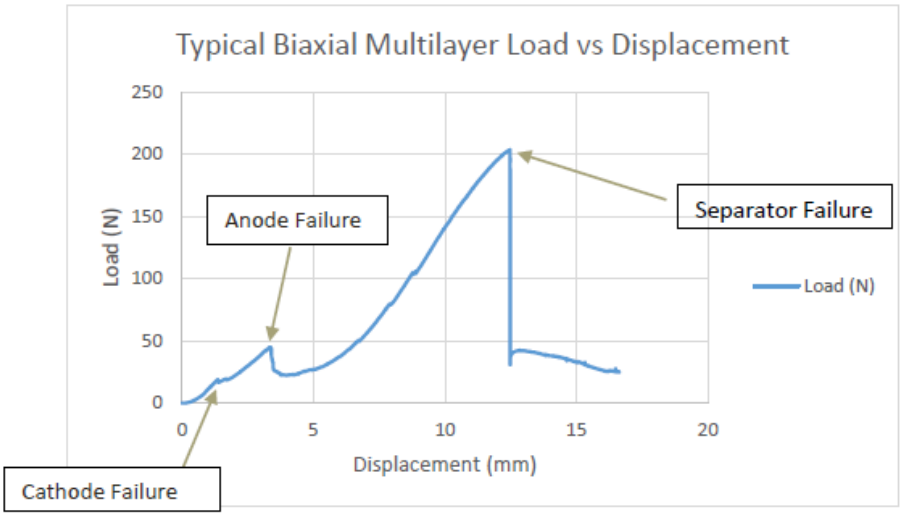

Figure 36 Load vs. Punch Travel 3 Layer Type B

Next, a representative specimen from each component of the single layer tests was chosen and their resistive loads were added together at each displacement. The resultant load vs displacement curve was then compared to the multilayer specimen graph as in Figure 37

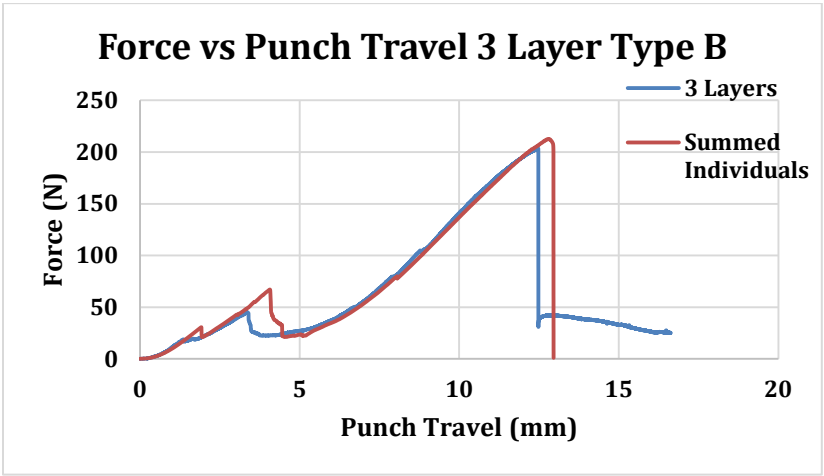

Figure 37 Summed Individual vs 3 Layer Biaxial Punch Tests Type B

As seen in the above figure, when the individual layers are added together, they are nearly identical to the 3 layer specimen. There are small differences in the breaking resistances most likely due to the increased friction from the interaction between layers in the multilayer specimen.

3.3.5 Biaxial Punch Tests with Short Circuit Detection

The author developed an innovative test to determine the onset of electric short circuit in a single multilayer specimen punch test. The benefit of this approach is that one doesn't need to use an entire battery to test for electric short circuit, and could therefore save money in testing. In the following subsections, the development of this method is detailed followed by the results. All tests described in this section were conducted on battery type B.

3.3.5.1 Component Conductivity Checks

Initially a series of conductivity checks were accomplished in order to further understand the electrical properties of the battery components.

Separator

As expected, the separator was not conductive to electricity. Furthermore, the separator material provided electrical insulation when an ohmmeter was connected to separate pieces of conductive material and the three layers were pressed on to each side of the separator. Figure 38 illustrates the electrical isolation properties of the separator material.

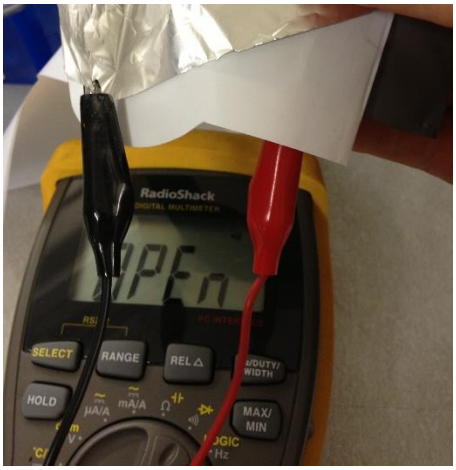

Figure 38 Separator Material Provides Electrical Insulation

Copper Anode

The copper anode consisted of copper metal covered on both sides by thin layer of carbon. Since carbon and copper are both conductive, it was predictable that when an ohmmeter is placed on separate ends of the anode there was an electric short circuit. Figure 39 demonstrates this property of the anode.

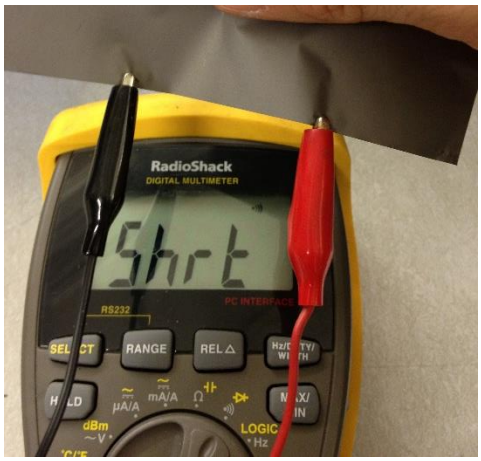

Figure 39 Anode Shows Conductivity to Electricity

Aluminum Cathode

The aluminum cathode consisted of aluminum metal covered on both sides by a thin layer of lithium cobalt oxide, or $LiCoO_2$. $LiCoO_2$ is not conductive to electricity, and the layer was thick enough such that it provided electrical insulation from the aluminum when connected to an ohmmeter. This property of the cathode is demonstrated in Figure 40.

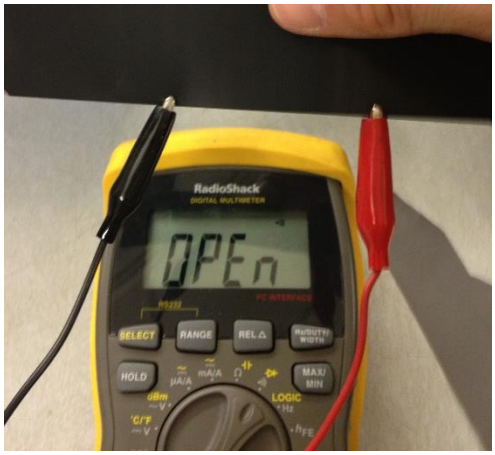

Figure 40 Cathode Shows Non-conductivity to Electricity

It is important to note here that if the $LiCoO_2$ coating was forcefully removed before the ohmmeter was attached, then the ohmmeter would display a short circuit due to the electricity traveling through the aluminum metal.

Multilayer Punch Test Specimen Preparation

In order to determine when short circuit occurs during a biaxial stress test, it was necessary to begin the test with complete electrical insulation between the anode and cathode. To achieve electrical insulation in the biaxial stress test fixture, specimen templates were developed in a computer aided design (CAD) program called Rhino. These templates allowed for electrical isolation in the testing fixture, as well as provide test points for connection to the ohmmeter. Figure 41, Figure 42, and Figure 43 illustrate the templates for the specimens.

Table 1 Legend for CAD Renderings

Material	Color
Separator	Yellow
Copper Anode	Red
Aluminum Cathode	Blue

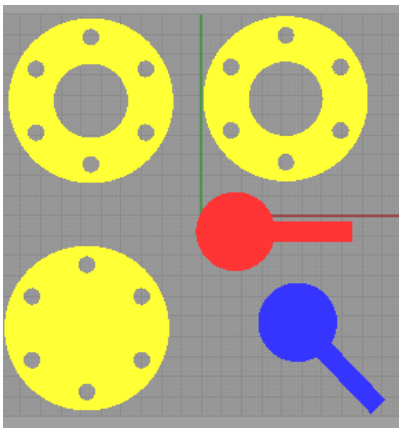

Figure 41 Biaxial Punch Test Specimen Templates

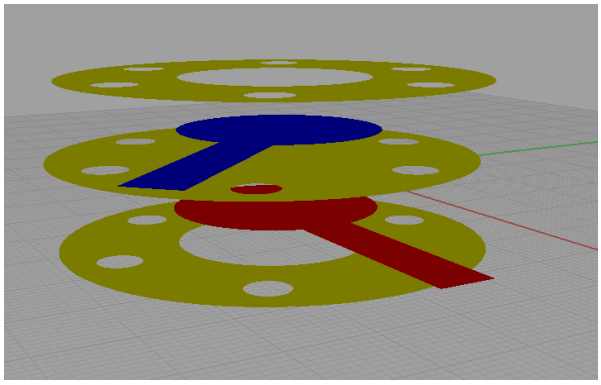

Figure 42 Biaxial Punch Test Specimen Templates in Stacked Position

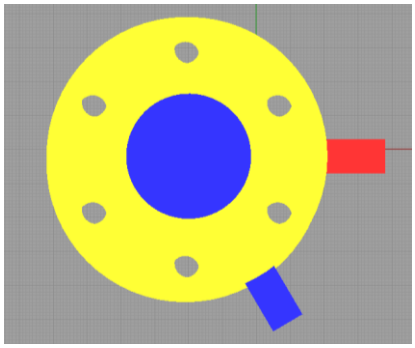

Figure 43 Biaxial Punch Test Specimen Templates in Stacked Position (Top View)

The templates were cut out using a Universal Laser Systems Versa Laser Cutting machine in the MIT Product Design Laboratory. The laser cutting machine was used to

ensure consistency at achieving electrical isolation in the template dimensions throughout the tests. Figure 44 illustrates the laser cutter performing cutting operations on a separator specimen.

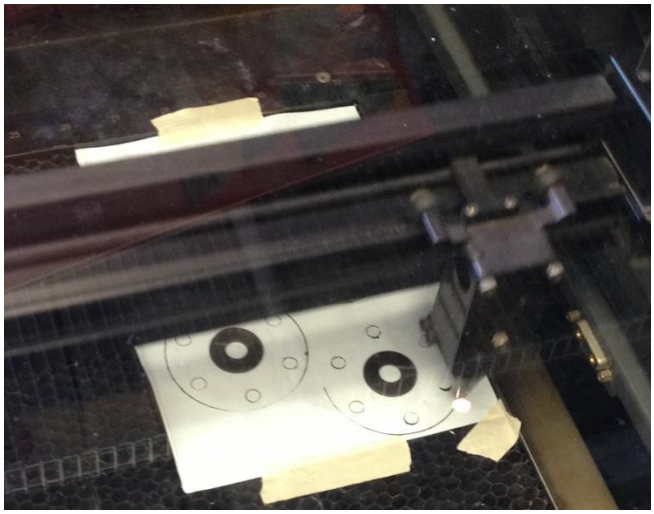

Figure 44 Separator Specimens Being Laser Cut

The laser cutting machine proved to do a satisfactory job for the biaxial punch tests, however it seemed to burn the edges of the material that it was cutting. This means that using a laser cutter for the uniaxial tests would not be recommended due to the interference of the burnt edges with the section of material that would be undergoing strain.

3.3.5.2 Biaxial Stress Tests 461-463

The development of the biaxial stress tests with the short circuit analysis was done on test numbers 461-463. It took four tests to develop the method enough so that it provided satisfactory results, which are described below along with the setup of the test.

The setup of the biaxial stress tests was conducted as mentioned in the previous section. Figure 45 shows the setup in the pre-test phase. Notice how the ohmmeter read "open" when connected to both the anode and cathode, demonstrating that we achieved electrical isolation of the cathode and anode.

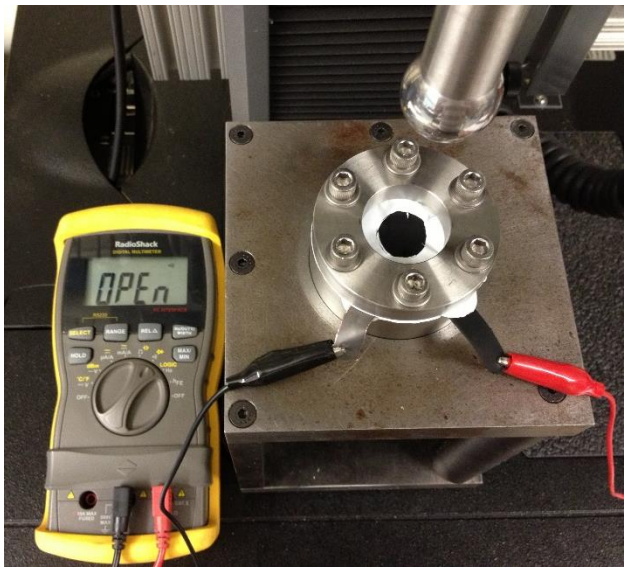

Figure 45 Biaxial Punch Test with Multi-meter

Test 461 was set up using dry specimens. The author's prediction was that short circuit may not be achieved due to the non-conductive properties of the Al cathode coating. In fact, after the mechanical failure of the separator in this test, there was no short circuit. The author could view the anode physically touching the cathode, and still there was no short circuit. The resultant force vs displacement graph of test 461 is shown in Figure 46.

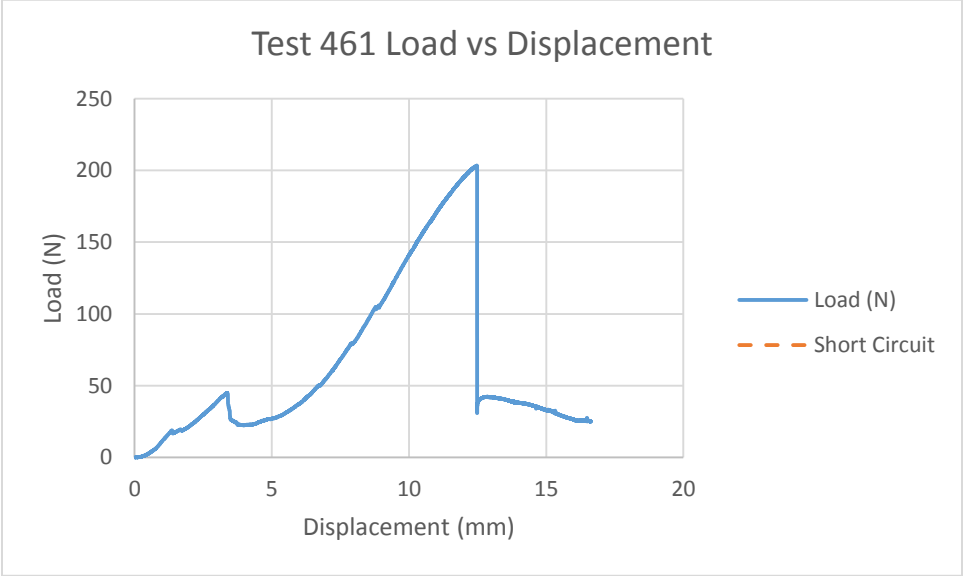

Figure 46 Test 461 Load vs Displacement

Test 462 was set up using wet specimens. The specimens were soaked in water for a period of 2 hours before they were placed in the test fixture. After the failure of the separator, short circuit did not occur for a number of minutes, so the authors returned the punch to the starting position. Once this happened, a short circuit occurred. The author's theory is that the quick release and rubbing of the punch on the cathode mechanically removed enough of the $LiCoO_2$ from the cathode to cause a short circuit. The resultant force vs displacement graph of test 461 is shown in Figure 47.

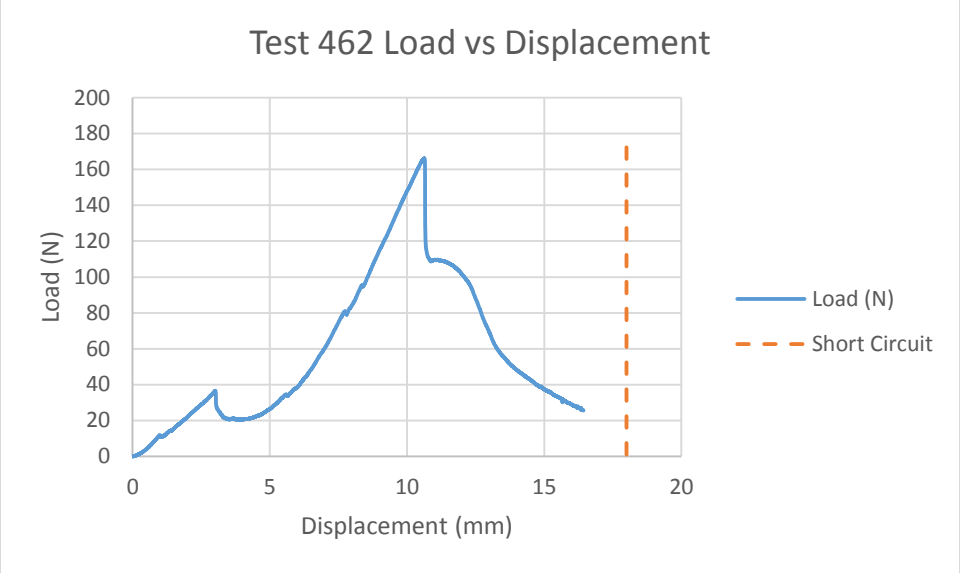

Figure 47 Test 462 Load vs Displacement

Test 463 was set up using wet specimens as was the case in test 462. The specimens were left in water for a period of 30 minutes. However, before being placed in the test fixture, the $LiCoO_2$ layer was removed from the aluminum cathode. The purpose of this test was to confirm the authors suspicions that the non-conductive properties of the $LiCoO_2$ were preventing short circuit. In the end, 784 seconds into the test, the separator had a mechanical failure and at 812 seconds into the test the ohmmeter registered a short circuit. The resultant force vs displacement graph of test 461 is shown in Figure 48.

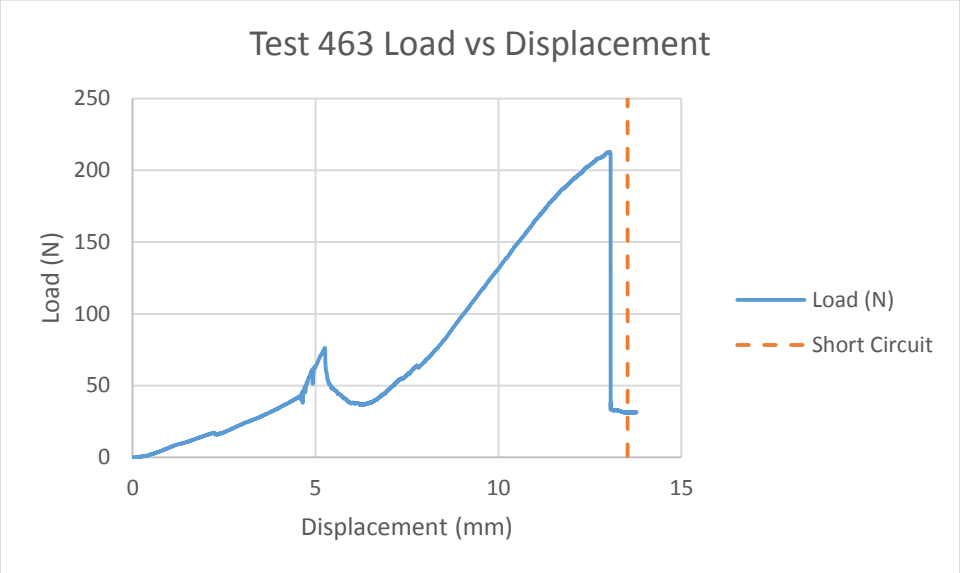

Figure 48 Test 463 Load vs Displacement

Test 464 was conducted in the exact same manner as 463. The reason for this test was to verify the results of the previous test. In the end, a short circuit occurred less than

a second after the mechanical failure of the separator. The resultant force vs displacement graph of test 461 is shown in Figure 49.

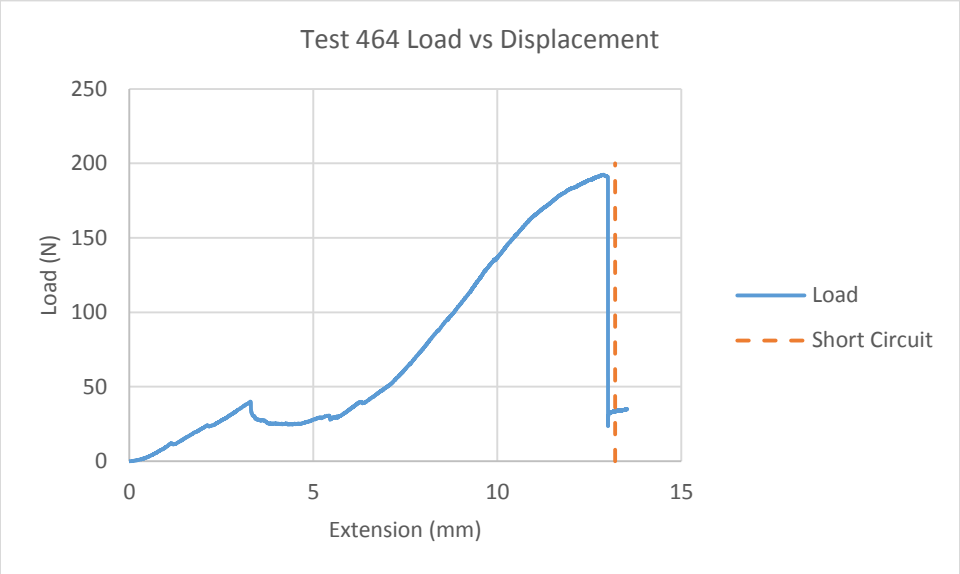

Figure 49 Test 464 Load vs Displacement

The final method used in experiments 463 and 464 seems to be reliable at showing that a short circuit occurs shortly after the mechanical failure of the separator. The variability in time for when the short circuit occurs can be attributed to the difference in failure areas of the 3 layers of material.

It is also important to note that in these experiments the separator material can support a much higher load than the anode or cathode without failure. The average breaking strength for the separator is 4 times the average breaking strength of the copper anode and 8 times the average breaking strength of the aluminum cathode. A graph outlining the typical breaking strengths of each material is shown in Figure 36.

3.3.6 Biaxial Multilayer Wet vs. Dry Tests

In an actual Li-ion battery, the component material is soaked in an electrolyte solution. An article published in the Journal of Power Sources claims that the differences in mechanical properties between a wet Li-ion battery separator and a dry separator are large enough to invalidate many results from testing using only dry separator material (Sheidaei, et al. 2011). In order to test this claim, the author acquired the main solution in battery electrolyte, Di-Methyl Carbonate (DMC), and soaked three multilayer specimen samples of type B in it for a period of twenty minutes. According to Sheidaei et al., twenty minutes is the minimum time needed to achieve full saturation of the separator material.

After soaking, the wet specimens were placed in the biaxial punch fixture in the order of, from top to bottom, Al cathode, separator, Cu Anode, and separator. The punch was

pushed through the multilayer specimens at a rate of 2mm/min. Additionally, three dry multilayer specimens from battery type B were tested for comparison with the wet specimens. The results of both the dry and wet specimen tests are shown in

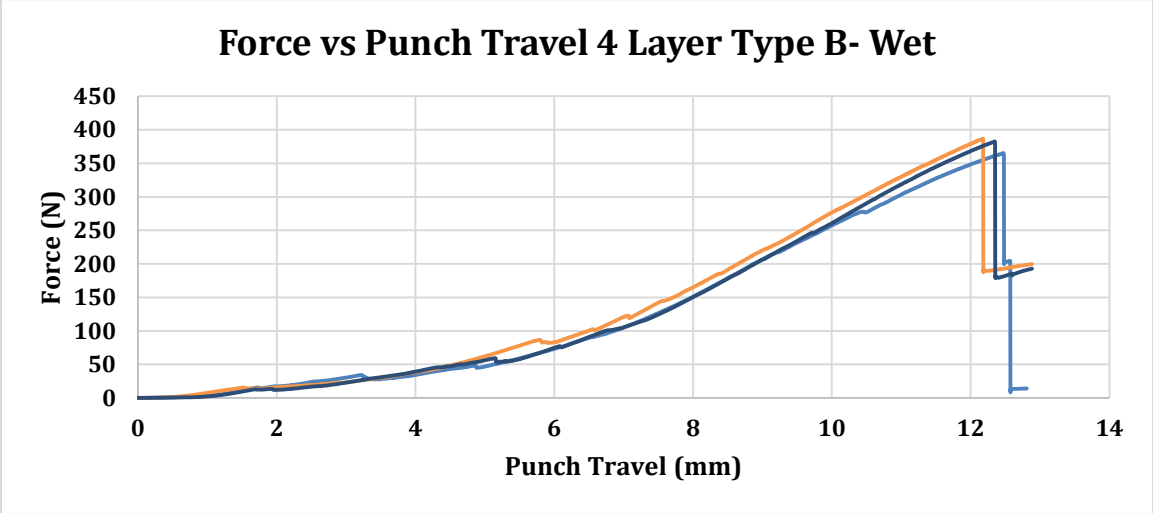

Figure 50 Force vs Punch Travel 4 Layer Type B- Wet

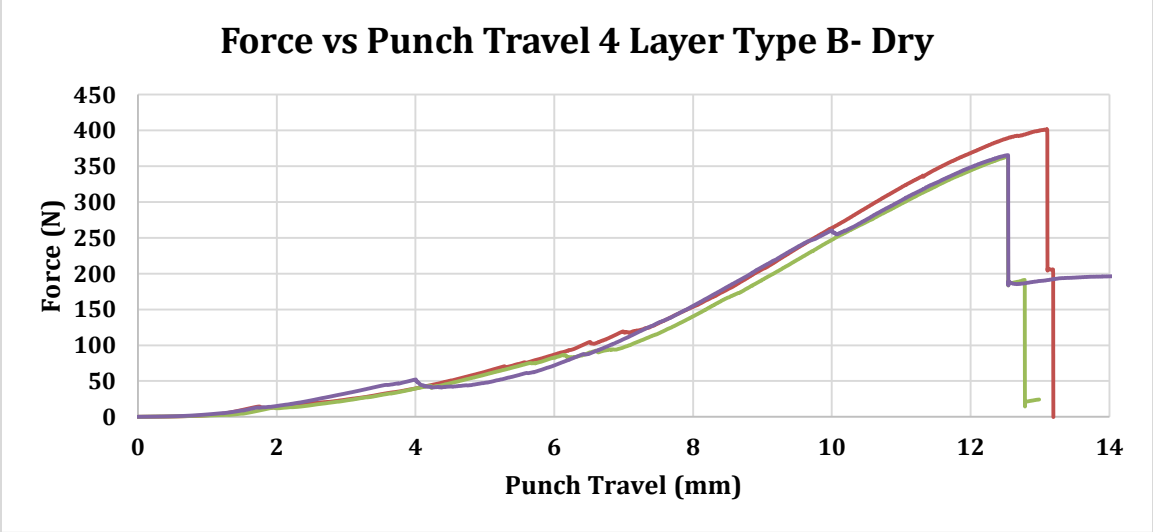

Figure 51 Force vs Punch Travel 4 Layer Type B- Dry

As seen in the above tests, both the wet and dry tests provided similar results. The average final breaking punch travel for the first layer of separator was approximately 12.5 mm for both the wet and dry specimen. The average force resistance seen at the first separator break was approximately 375 N for both specimen types.

These test results do not necessarily disprove the previous findings, however, more research is needed to understand the exact mechanical property differences for wet and dry battery material specimens.

3.4 Micro-Mechanical Observations through Electron Microscopy

Following the uniaxial and biaxial tensile testing of the battery component material, the author then was trained by the Center for Materials Science and Engineering (CMSE) at MIT in the use of their FEI/Philips XL30 scanning electron microscope. The author utilized this microscope to take pictures of different battery components in order to better understand the tests results mentioned in the previous sections. The following sections display the different pictures that the author was able to take along with some interesting observations that can be drawn from each picture.

3.4.1 Picture Orientation Nomenclature

In order to orient the reader for viewing pictures in the following sections, a CAD model representing an example sheet of battery component was created. Figure 52, Figure 53, and Figure 54 show the different orientation nomenclature that are maintained throughout this section of the study.

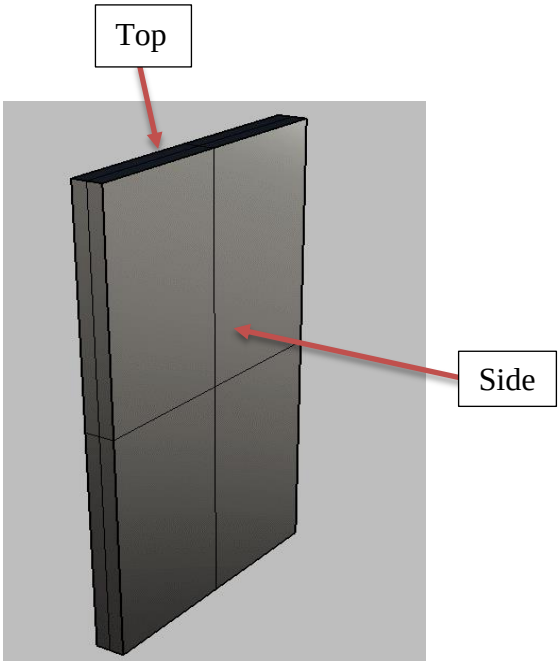

Figure 52 Battery Component 3D Representation

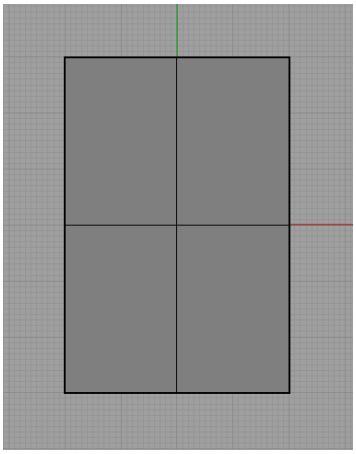

Figure 53 Battery Component Side View

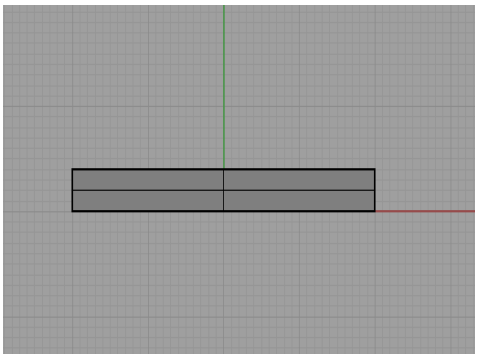

Figure 54 Battery Component Top View

3.4.2 Type A Battery SEM

The first type of battery looked at using the SEM was the type A battery. The following specimens were cut out with the same type of X-acto knife as was used in the uniaxial stress tests. Once cut, the specimens were secured to an observation disk with tape for viewing. Great care was taken during the specimen preparation process to ensure minimal damage to the specimen during handling.

3.4.2.1 Uncoated Aluminum

A sample of uncoated aluminum was obtained from the manufacturer of type A Li-ion batteries. It was confirmed via phone call that this was the same size and makeup of material that was used in the production of the Al cathode. The purpose of this picture was to understand how much damage was done to the material in its production.

Figure 55 shows a side view of the uncoated aluminum. As seen in the picture, there seem to be very few manufacturing defects in the material. These small imperfections could be correlated with the small disparity in breaking displacement between Type A aluminum specimens.

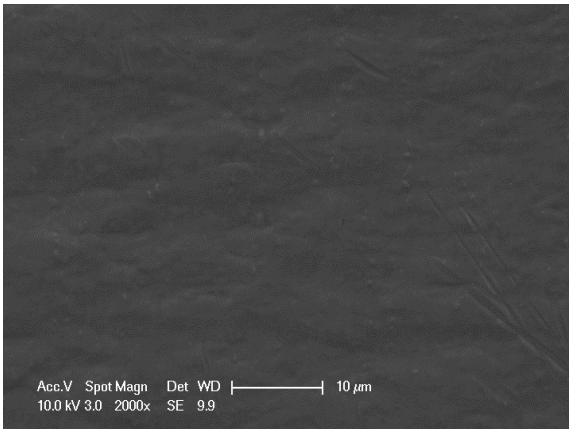

Figure 55 Uncoated Al Side View

Next the author took a photograph of the uncoated Al from the top as shown in Figure 56. The notable feature of this photograph is the damage done to the top edge of the material. This is significant to note because this edge was not tampered with by the author, but was the edge cut in the manufacturing process.

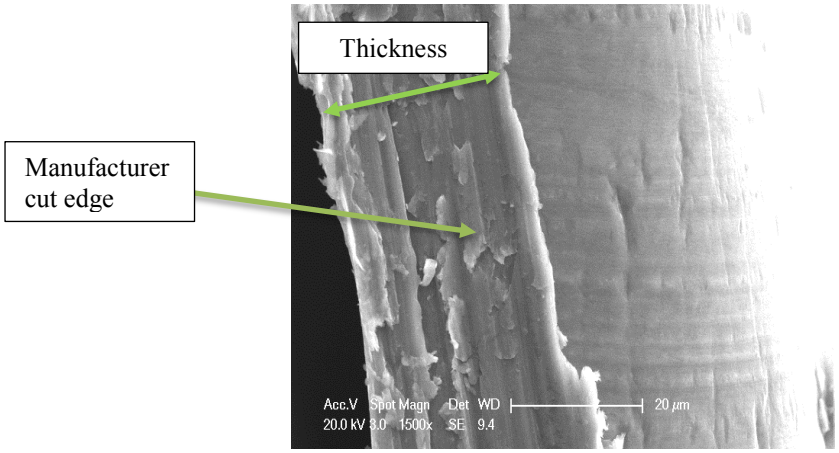

Figure 56 Uncoated Aluminum Top View

3.4.2.2 Uncoated Copper

Next a sample of uncoated copper was obtained from the manufacturer of type A Li-ion batteries. It was confirmed via phone call that this was the size and make of material that was used in the production of the Cu anode. The purpose of these type pictures was to understand how much damage was done to the material in its production, as well as to better understand the effect that the coating process has on the mechanical properties of the material.

Figure 57 shows a side view of the uncoated copper. In the image, it is apparent that there are large imperfections in the specimen compared to the Al. These imperfections are most likely due to the manufacturing processes used to make the copper sheet. These

large imperfections could be correlated with the disparity in break extension between type A copper specimens.

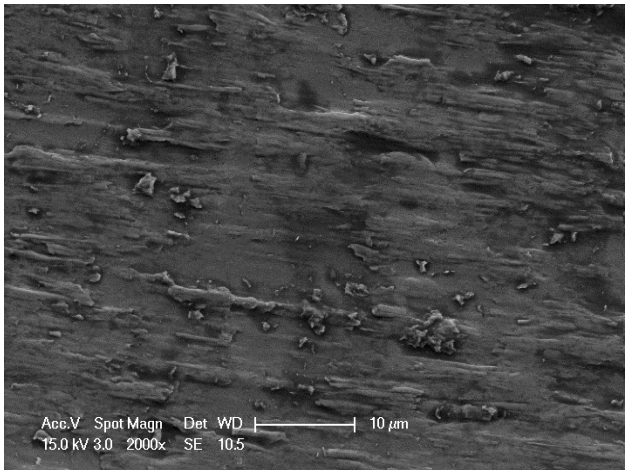

Figure 57 Uncoated Copper Side View

Next the author took a photograph of the uncoated Cu from the top as shown in Figure 58. The notable feature of this photograph is the apparent smooth surface of the manufacturer's cut edge of the specimen. This edge appears smoother than the edge of the aluminum material.

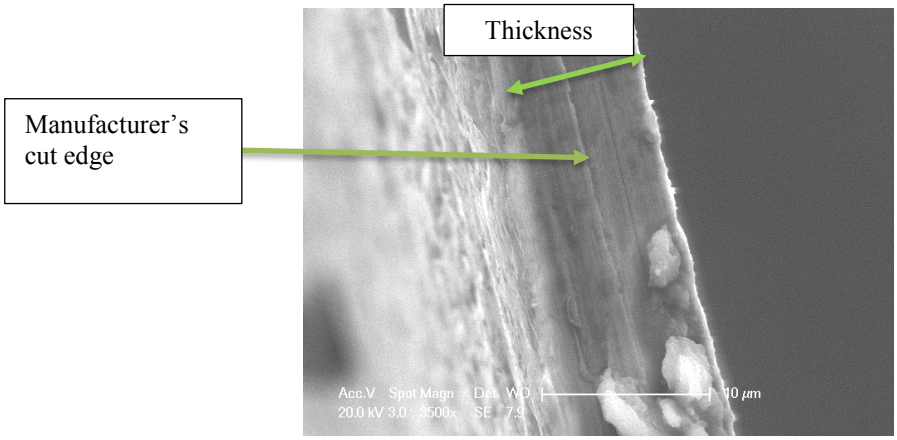

Figure 58 Uncoated Copper Top View

3.4.2.3 Coated Aluminum

Photographs of the coated Al cathode were taken in Figure 59, Figure 60, Figure 61, and Figure 62. The first two photographs were taken in a side view configuration at varying zoom magnitude and show the $LiCoO_2$ coating on the aluminum. It is interesting to see how the coating is able to prevent the formation of the Li dendritic structures by allowing forcing the Li-ions to separate before moving to the Al metal.

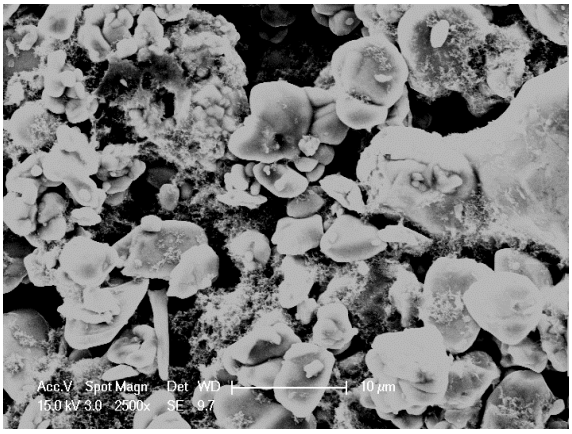

Figure 59 Coated Aluminum Side View

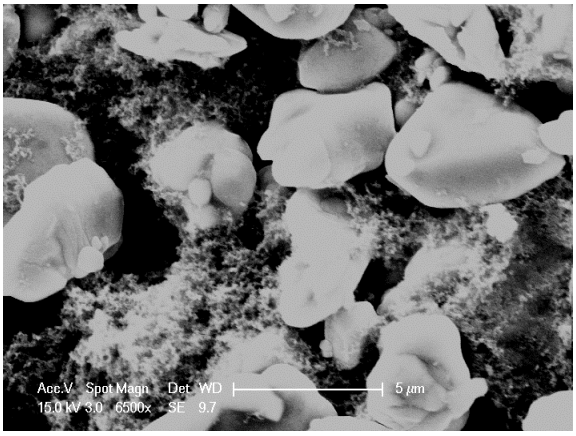

Figure 60 Coated Aluminum Side View

Figure 61 and Figure 62 show top views of the Al cathode. These views allowed the author to visualize the coating attached to the Al sheet. Additionally, they allowed the author to understand the effects of cutting the specimen with an Xacto knife. As can be seen below, the coating is securely attached to the aluminum sheet in the manufacturer's cut edge, but in the Xacto cut edge the separator is beginning to detach from the metal.

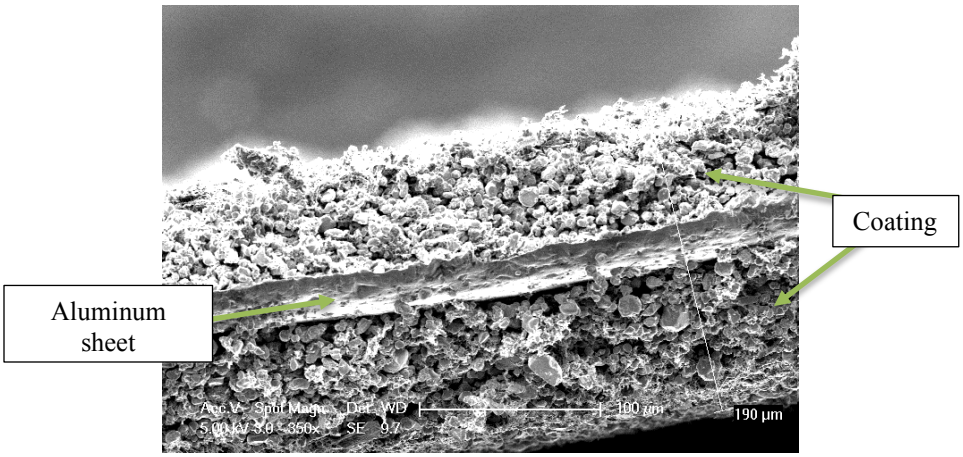

Figure 61 Coated Aluminum Top View

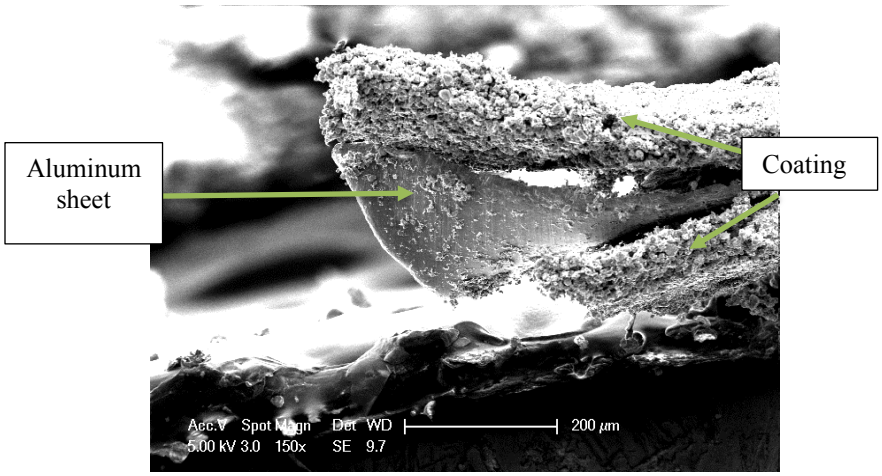

Figure 62 Coated Aluminum Top view (corner)

3.4.2.4 Coated Copper

Photographs of the coated Cu anode were taken in Figure 63
Figure 64, and Figure 65. The first photograph was taken in a side view configuration at a zoom of 10 µm and shows the carbon coating on the copper. It is interesting to see how the coating is able to prevent the formation of the Li dendritic structures by allowing forcing the Li-ions to separate before moving to the Cu metal.

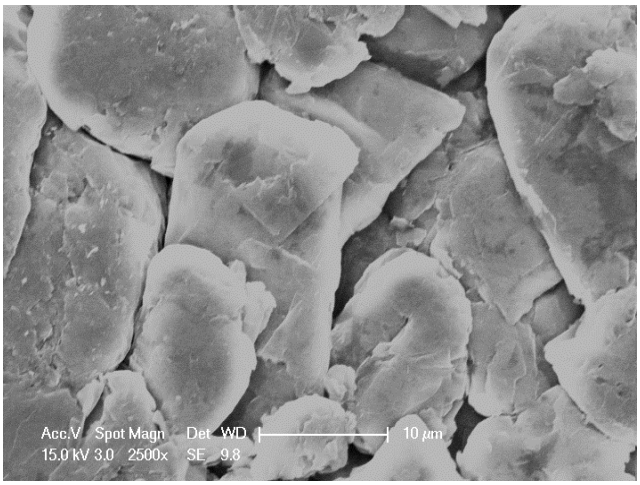

Figure 63 Coated Copper Side View

Figure 64 shows a top views of the coated Cu anode. It is interesting to observe that the manufacturer's edge displayed in this photograph appears show **unequal thicknesses** of coating on either side of the copper. Additionally, as with the Al cathode, the coating along this edge seems to have good cohesion to the metal sheet.

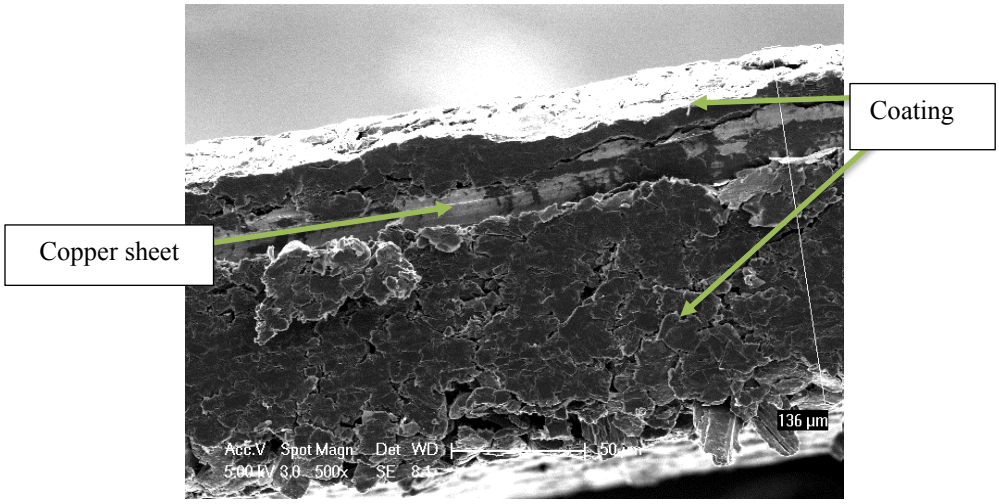

Figure 64 Coated Copper Top View

Figure 65 shows another top view of the coated Cu anode, however this view provides some insight as to what happens when an X-acto knife is used in specimen preparation. As seen in the below figure, the edge that was cut using an X-acto knife appears to have some separation between the metal and coating. Additionally, it appears in this photo that the edge of the copper is bent along the manufacturer's edge. This fact seems to explain the appearance of an uneven thickness of coating on either side of the metal sheet seen in Figure 64.

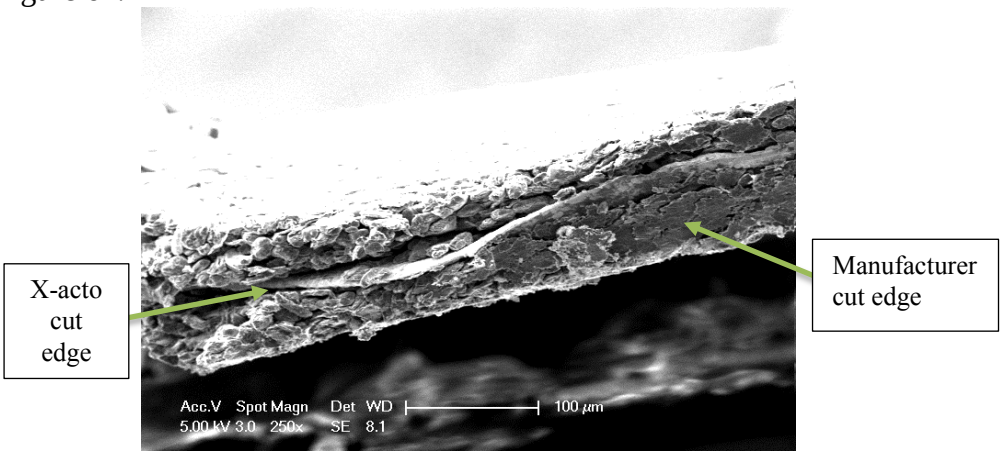

Figure 65 Coated Copper Top View (Corner)

3.4.2.5 Separator

The separator material of battery type A was photographed using a SEM. As seen in previous sections of this report, this separator material was shown to exhibit severe anisotropic properties in that it provided very low mechanical resistance in the TD compared to the MD. The author speculated in an earlier section that this separator was made using a dry method and was stretched in the TD during the manufacturing processes. As seen in Figure 66 and Figure 67, holes in the separator material appear to be aligned in a specific direction, indicating that a stretching step was used in the manufacturing of this material. Also, when compared to the separator of the type B

material, is seems that the holes in the type A separator are much larger and would allow for a more power dense battery.

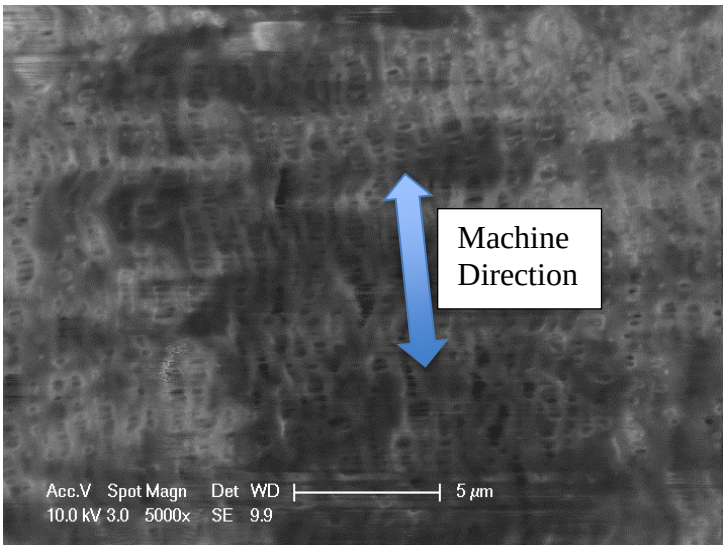

Figure 66 Separator Side View

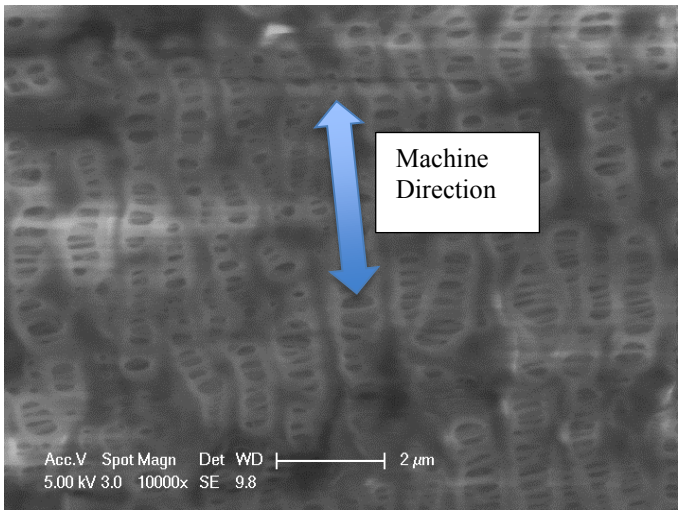

Figure 67 Separator Side View

3.4.3 Type B Material

The next type of battery tested was the type B battery. These specimens were cut out with the same X-acto knife as was used in the uniaxial stress tests. Once cut, the specimens were secured to an observation disk with tape for viewing. Great care was taken during the specimen preparation process to ensure minimal damage to the specimen during handling.

3.4.3.1 Coated Aluminum

Figure 68 shows a top views of the Al cathode. This picture shows an edge that would be created during the battery manufacturing process and is interesting because the metal

sheet is not visible from this view. When coated, the metal is surrounded even on the edges by the $LiCoO_2$. Also interesting to note is the strait surface along the edge. When comparing this edge with and edge cut out with an X-acto knife, such as in Figure 69, it is apparent that the knife has disturbed the metal-coating interface.

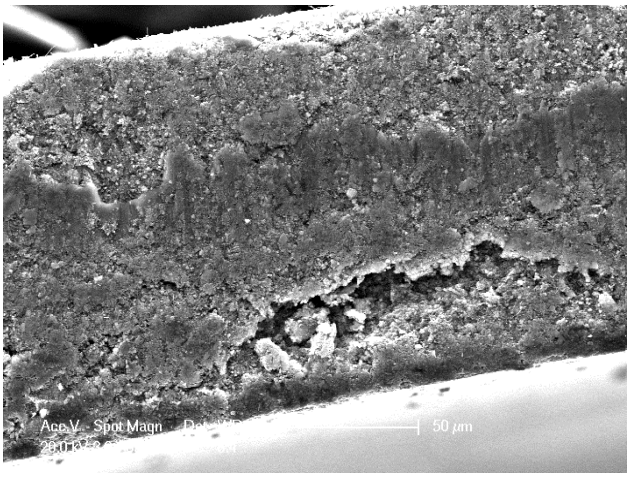

Figure 68 Coated Aluminum Top View

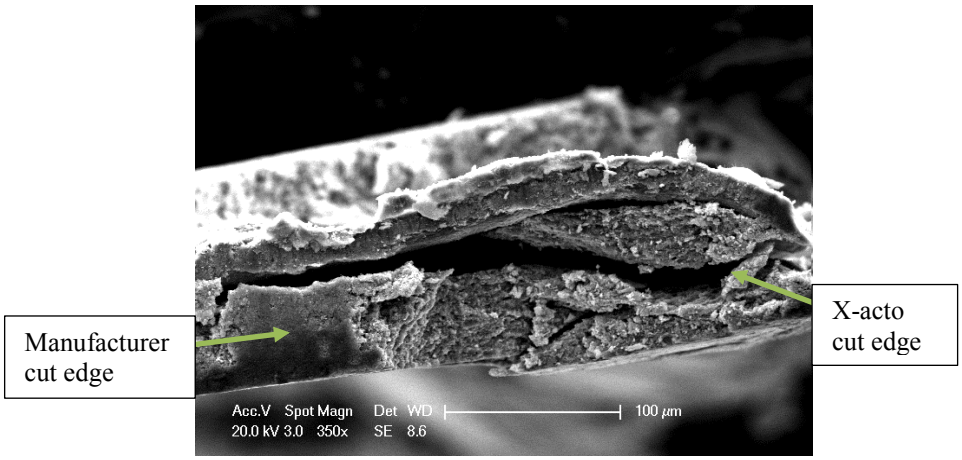

Figure 69 Coated Aluminum Top View (Corner)

3.4.3.2 Coated Copper

Next the coated copper anode of the type B material was observed with the SEM. As seen in Figure 70 and Figure 71 this type of coated copper looks very similar to the type A material. The thicknesses of the coating and metal are also similar to the type A material.

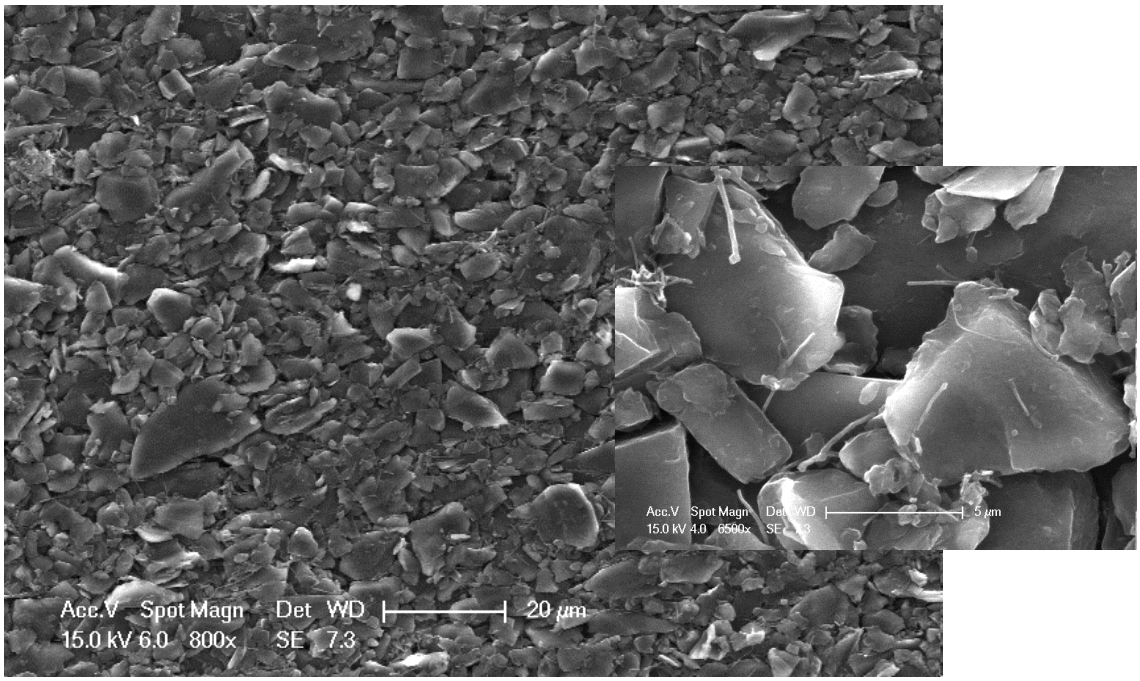

Figure 70 Coated Copper Side View (Zoomed in on Right))

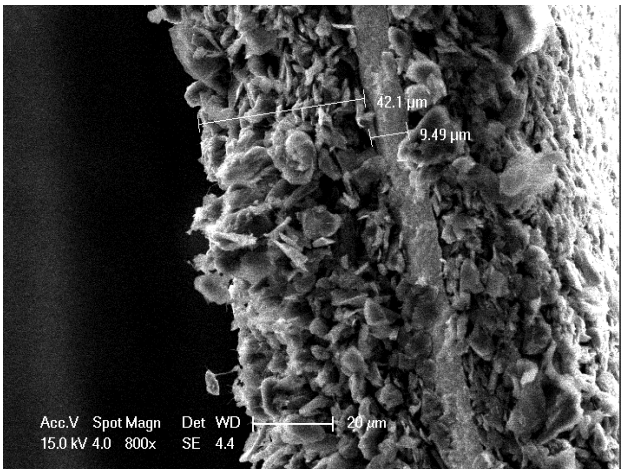

Figure 71 Coated Copper Top View

3.4.3.3 Separator

Figure 72 and Figure 73 show a side view of the separator material. These views are interesting beause the holes in this separator material are not visible. At the same scale, and with the same microscope, the separator material from the other type of battery is visible. The author hypothesiszes from the images below, that this material is manufactured using a wet process. This process would allow the separator to have the better mechanical characteristics it displays in the uniaxial and biaxial tests.

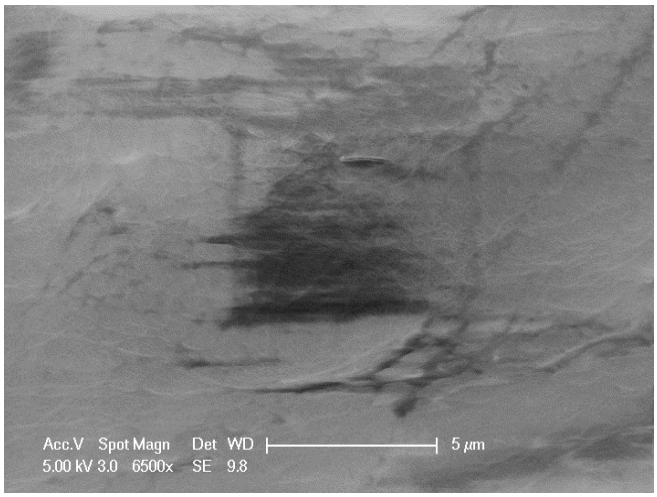

Figure 72 Separator Side View

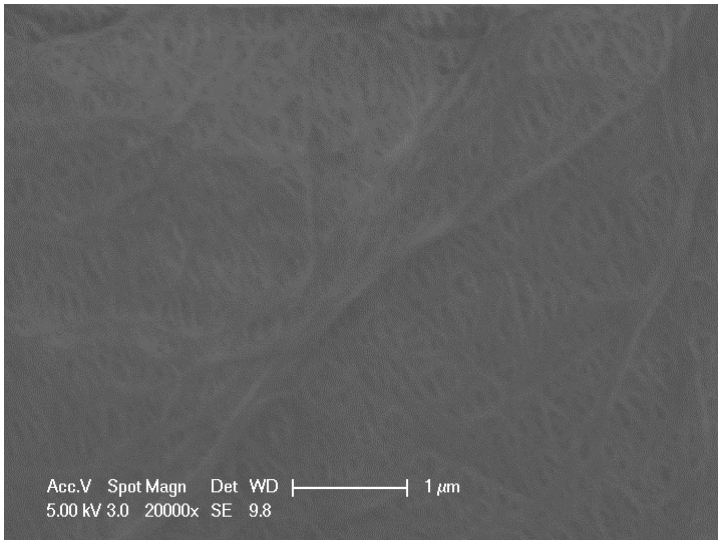

Figure 73 Separator Side View

Further efforts were made to view the holes in this separator material, but all proved unsuccessfull. In future iterations of aquiring SEM photographs for this material, it should be coated with some type of conductive spray. This step would reflect the electrons within the microscope back to the scanner and allow the author to view the holes.

3.4.4 Manufacturing Defects Viewed with SEM

After all of the battery specimens from both types of batteries had been observed in the SEM, the author was interested to view the metal sheet that was in the coated aluminum cathode. To remove the coating from the aluminum, the Al cathode was placed in a jar of water for 3 minutes. The specimen was then removed and the coating was removed by hand. It is important to note that no effort was needed to remove the coating and it slipped off effortlessly when soaked in the water. After the coating was removed, the specimen was softly patted with a paper towel to remove the water droplets before

observation with the SEM. Figure 74 shows the previously coated specimen as well as an uncoated specimen of aluminum.

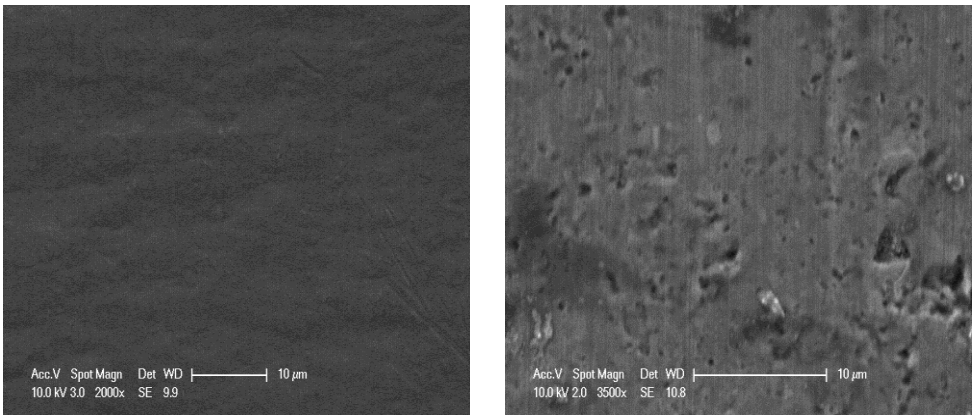

Figure 74 Bare Aluminum (Left) and Previously Coated Aluminum (Right)

As seen in the figure above, the bare aluminum is smooth and has very little imperfections. When shown at the same scale, the previously coated aluminum has large imperfections. These imperfections could be created during the coating process of the Al cathode, and could be why the bare aluminum sheet provides more resistance in the uniaxial tests than the Al cathode.

3.4.5 Partially Damaged Specimens

Once the breaking displacements of the type B battery components were known from the biaxial tests, four specimens of each electrode and separator were punched to ¼, ½, ¾ and full breaking displacement and then released. The specimens were then placed in a SEM and observations were made about their appearance. All specimens were photographed on the opposite side that the force was applied.

3.4.5.1 Aluminum

Figure 75 shows the Al cathode from the type B battery after it had been to ¼, ½, ¾ and full breaking displacements. Notice that the ¼ specimen hasn't developed any cracks in the coating yet. After the specimens were brought to ½ breaking displacement, cracks started to develop in the coating. No trend as to the size of the cracks versus their tested displacement could be observed after the cracks started to appear, therefore the resolution of the SEM photographs is not maintained the same throughout the images. The appearance of cracks before the expected plastic deformation could help to explain the large amount of noise seen in the DIC data for these specimens. When the DIC data is processed, it determines strain through the separation of small points of speckled paint on the material. If the coating of the material is cracking during the tests, then the DIC processing software would have a hard time calculating strain.

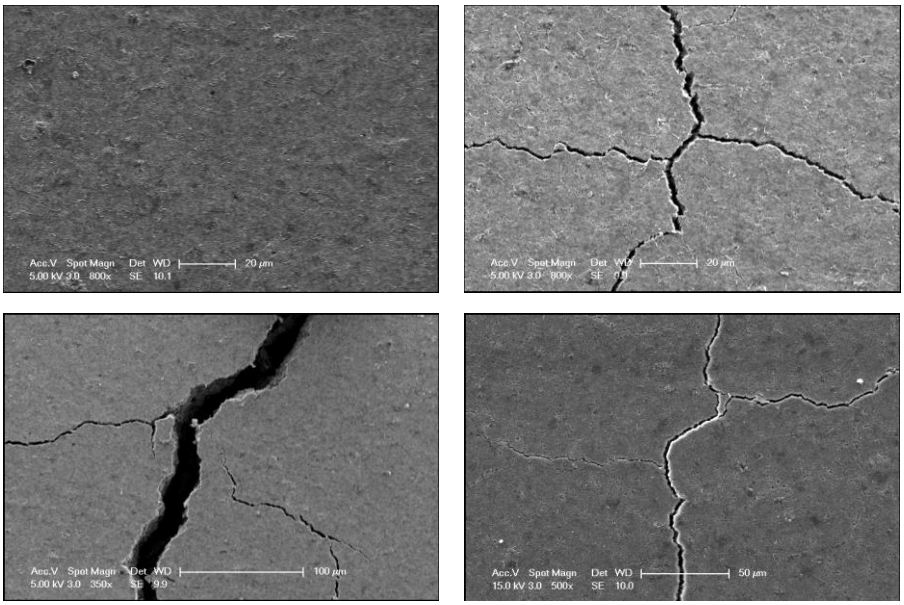

Figure 75 Al Cathode at 1/4 (Top Left), 1/2 (Top Right), 3/4 (Bottom Left), and Full (Bottom Right) Breaking Displacements

3.4.5.2 Copper

Figure 76 shows the Cu anode from the type B battery after it had been to ¼, ½, ¾ and full breaking displacements. Notice that the ¼ and ½ specimen haven't developed any cracks in the coating yet. After the specimens were brought to 3/4 breaking displacement, cracks started to develop in the coating. No trend as to the size of the cracks versus their tested displacement could be observed after the cracks started to appear therefore the resolution of the SEM photographs is not maintained the same throughout the images. When the DIC data is processed, it determines strain through the separation of small points of speckled paint on the material. If the coating of the material is cracking during the tests, then the DIC processing software would have a hard time calculating strain.

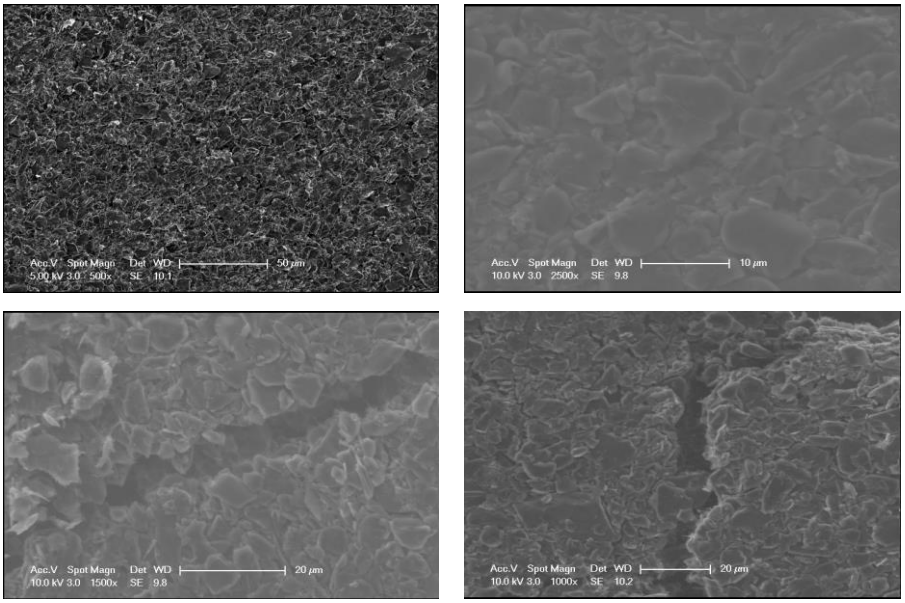
Acc.V Spot Magn Det WD 50 µm
5.00 kV 3.0 500x SE 10.1
Acc.V Spot Magn Det WD 10 µm
10.0 kV 3.0 2500x SE 9.8
Acc.V Spot Magn Det WD 20 µm
10.0 kV 3.0 1500x SE 9.8
Acc.V Spot Magn Det WD 20 µm
10.0 kV 3.0 1000x SE 10.2

Figure 76 Cu Anode at 1/4 (Top Left), 1/2 (Top Right), 3/4 (Bottom Left), and Full (Bottom Right) Breaking Displacements

3.4.5.3 Separator

Figure 77 shows the separator material from the type B battery after it had been to ¼, ½, ¾ and full breaking displacements. The ¼ breaking displacement figure looks similar to a non-damaged image of the separator. After the separator is brought to ½ breaking displacement the specimen is seen to have some permanent deformation where the punch was pressing. At ¾ and full breaking displacement the separator has thinned so that the specimen holding dish is starting to reflect light through the separator material. More defined SEM photos should be taken of this material in order to understand what is actually occurring with the fibers.

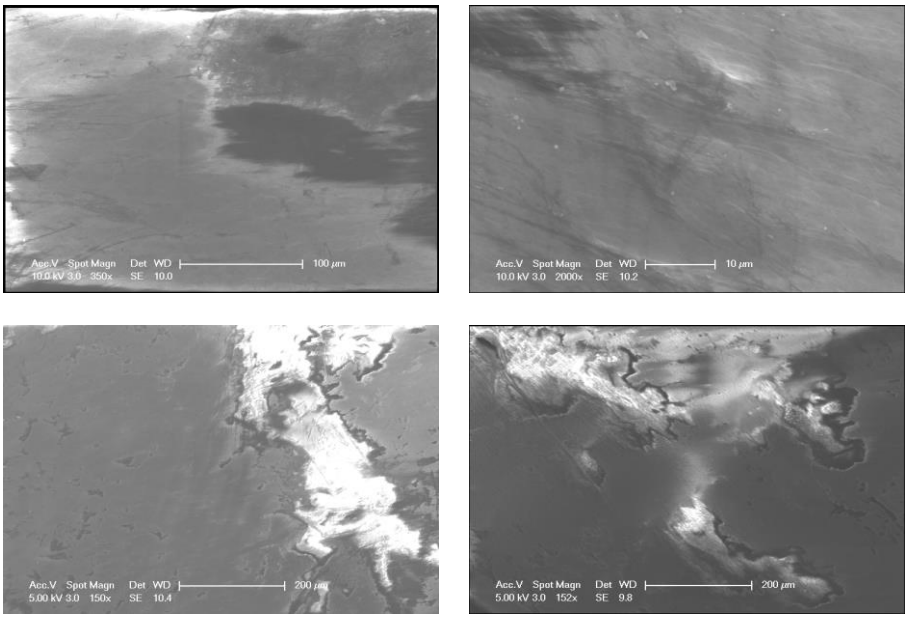
Acc.V Spot Magn Det WD 100 µm
10.0 kV 3.0 350x SE 10.0
Acc.V Spot Magn Det WD 10 µm
10.0 kV 3.0 2000x SE 10.2
Acc.V Spot Magn Det WD 200 µm
5.00 kV 3.0 150x SE 10.4
Acc.V Spot Magn Det WD 200 µm
5.00 kV 3.0 152x SE 9.8

Figure 77 Separator Material at 1/4 (Top Left), 1/2 (Top Right), 3/4 (Bottom Left), and Full (Bottom Right) Breaking Displacements

4.0 Conclusions

Lithium-ion battery components have been characterized throughout this work in over 200 tests using various testing methods. From these results, the author has made several conclusions about the mechanical characteristics of the electrode and separator material properties as well as how these components might behave inside of a fully functional battery pouch.

The separator material can sustain a much larger strain before failure than either the Cu anode or Al cathode. This fact has been shown throughout the uniaxial and biaxial tests. Also, it has been shown in this research that, in an actual Li-ion battery, once the separator fails, an internal short circuit is likely to occur immediately after.

The separator material from type A and type B are most likely manufactured using different methods. When viewing both materials through a SEM, the holes in the type A battery are much larger and more aligned than those of type B. The uniaxial and biaxial tension tests demonstrate the severe anisotropic properties of the type A separator. Although it is true that type B separator is anisotropic as well, it is much less anisotropic than type A.

The varying strain rate tests demonstrate how the type B separator material exhibits different mechanical properties when the speed of the test is altered. As the test speed increases, so does the separator stress for a given strain. Now that this property of the

separator has been characterized, it can be incorporated into the FEA models in order to refine them.

The uniaxial tests show that the electrode metals are weaker than the uncoated metals of the same makeup and size. When viewed with a SEM, the surface of the Al cathode stripped of its coating had large imperfections while the bare Al metal sheet had a smooth surface. This damage most likely occurs during the coating process of manufacturing the electrodes.

Most of the SEM photos show that specimens cut out with an X-acto knife seemed to have damage the metal/coating boundary of that specimen. This could have a minor impact on the uniaxial component tests currently being conducted by the ICL, but not to the biaxial.

5.0 Future Work

These results will be used to further refine and validate a high-level, robust, and accurate computational tool to predict strength, energy absorption, and the onset of electric short circuit of batteries under real-world crash loading situations. The cell deformation models will then be applied to the battery stack and beyond, thereby enabling rationalization of greater optimization of the battery pack/vehicle combination with respect to tolerance of battery crush intrusion behavior. Besides improving crash performance, the finite element models contribute substantially to the reduction of the cost of prototyping and shorten the development cycle of new electric vehicles.

There are also more tests that could be run on these same battery components in order to refine the FEA model further than this work has accomplished. True stress vs strain data is difficult to capture when testing the electrodes since both the coating and metal move differently. Further work should attempt to understand how the interactions of these layers occur. Once this is understood, true stress vs strain data can be determined using existing equipment for both the biaxial and uniaxial tests.

Finally, SEM work should continue if new testing methods are developed or if new battery types are acquired by the ICL for testing. The photographs taken in this work were crucial in understanding the uniaxial and biaxial tests, as well as determining what types of tests should be conducted in the future.

Appendix A List of Acronyms and Abbreviations

Al	Aluminum
ASME	American Society of Mechanical Engineers
CMSE	Center for Material Science and Engineering
Cu	Copper
DIC	Digital Image Correlation
DMC	Di-Methyl Carbonate
FEM	Finite Element Model
ICL	Impact and Crashworthiness Laboratory
kN	Kilonewton
Li-Ion	Lithium Ion
Lp	Parallel Length (of test specimens)
MD	Machine Direction
MIT	Massachusetts Institute of Technology
N/mm^2	Newtons per millimeter squared
RVE	Representative Volume Element
SEM	Scanning Electron Microscope
TD	Transverse Direction
μm	Micro Meters

References

ASME. 2001. *Guidelines for Pressure Boundary Bolted Flange Joint Assembly.* American National Standard, New York City: American Society of Mechanical Engineers.

Campbell, John. 2012. *Development of a Constitutive Model Defining the Point of Short Circuit Within Lithium-Ion Battery Cells.* Cambridge: Massachusetts Institute of Technology.

Gwon, S.J., J.H. Choi, and J.Y. and et al. Sohn. 2009. "Preparator of a new micro-porous poly(mehyl methacrylate)-grafted polythylene separator for high performance Li secondary battery." *Nuclear Instruments and Methods in Physics Research B* 3309-3313.

Hill, Richard. 2011. *Development of a Representative Volume Element of Lithium-Ion Batteries for Thermo-Mechanical Integrity.* Cambridge: Massachusetts Institute of Technology.

Jeon, M.Y., and C.K. Kim. 2007. "Phase Behavior of Polymer/diluent/diluent Mixtures and Their Application to Control Microporous Membrane Structure." *Journal of Membrane Science* 3309-3313.

Meier, Joseph D. 2013. *Material Characterization of High-Voltage Lithium-Ion Battery Models for Crashworthiness Analysis.* Cambridge: Massachusetts Institute of Technology.

Sahraei, Elham, Richard Hill, and Tomasz Wierzbicki. 2011. "Calibration and Finite Element Simulation of Pouch Lithium-Ion Batteries for Mechanical Integrity." *Journal of Power Sources* no.

Sahraei, Elham, Richard Hill, and Tomasz Wierzbicki. 2010. "Homogenized constitutive model of the cylindrical lithium-ion battery cell." *Journal of Power Sources* no.

Sheidaei, Azadeh, Xinran Xiao, Xiaosong Huang, and Jonathon Hitt. 2011. "Mechanical behavior of a battery separator in electrolyte solution." *Journal of Power Sources* 8728-8734.

Wierzbicki, Tomasz, and Elham Sahraei. 2013. *4th MIT Workshop on Computational Modeling of Lithium-Ion Batteries.* Battery Consortium Proceedings, Cambridge: Massachusetts Institute of Technology, 19.

Wierzbicki, Tomasz, Elham Sahraei, and Richard Hill. 2011. "Lithium Ion Cells with Experimental Validation." *Journal of Power Sources* S.1.

Zhang, S.S., M.H. Ervin, and K., Jow, T.R. Xu. 2004. "Microporous polyacrylonitrile-methyl methacrylate membrane as a separator of rechargeable lithium battery." *Electrochimica Acta* 3339-3345.